Marine Chemistry 211 (2019) 75–93

Contents lists available at ScienceDirect

Marine Chemistry

journal homepage: www.elsevier.com/locate/marchem

Particulate organic matter distributions in surface waters of the Pacific Arctic shelf during the late summer and fall season

Miguel A. Goñi*, Elizabeth R. Corvi, Kylie A. Welch, Maggie Buktenica, Kaitlin Lebon, Yvan Alleau, Laurie W. Juranek

College of Earth, Ocean & Atmospheric Sciences, Oregon State University, Corvallis, OR 97331, USA

ARTICLE INFO

Keywords:
Particulate organic carbon
Carbon/nitrogen ratio
Polar waters
Western Arctic
Northern Bering Sea
Chukchi Sea

ABSTRACT

Climate change is leading to marked decreases in the extent, thickness and persistence of sea ice in Polar Regions, especially during the later summer and fall seasons. The expanded open water domain during this period has the potential to drastically affect the hydrography, biogeochemistry and ecology of Arctic seas. In view of these rapid changes, the distributions of particulate organic matter in surface waters from the Pacific Arctic shelf were determined during the late summer and early fall months (August–October) over four different years (2012, 2015, 2016, and 2017). Utilizing surface underway systems of research vessels in combination with a semi-automated filtration system, over a thousand individual samples from surface waters were collected along the northern Bering Sea and Chukchi Sea shelves. Particulate organic carbon (POC) concentrations and molar carbon:nitrogen ratios ([C:N]) were determined to investigate the distribution and provenance of organic matter in surface waters at a high spatial resolution along the research vessels' navigational paths. Corrections for sorption of dissolved carbon and nitrogen were possible at high frequency because of our sampling techniques. The resulting blank-corrected POC concentrations in surface waters ranged from < 2 to 35 μM, with several samples collected earlier (August) in the open water season displaying much higher concentrations (> 60 μM). Large spatial and temporal variability characterized measurements throughout the study area, with maxima in POC concentration often measured in association with physical features (e.g., straits, capes, fronts, shoals) and strong wind events. Hydrographically, POC distributions displayed significant variability among water masses in the region. Alaska Coastal Water, which was predominant along the southern section of the study area (between Bering Strait and Pt. Hope), displayed the highest POC concentrations whereas Bering-Chukchi Shelf Water and especially Melt Water, which occupied the northern section of the study area (Pt. Hope to Utquiagvik) were characterized by the lowest POC concentrations. Earlier periods (August–September) also were characterized by higher average POC concentrations than later periods (September–October). Overall, most of the samples collected exhibited [C:N] ratios that ranged from 6 to 8 mol:mol, and were consistent with a predominant marine provenance. Our findings indicate POC distributions reflect patterns of wind forcing and physical circulation and identify regions of localized high standing stocks that suggest spatially and temporarily variable production in this area during the late open-water season.

1. Introduction

Warming associated with increased atmospheric CO_2 concentrations has led to significant decreases in ice cover and sea ice thickness throughout the Arctic Ocean (e.g., Fetterer et al., 2017; Wood et al., 2015; Vaughan, 2013). The rapid and marked reduction in ice cover and sea ice thickness has the potential to dramatically affect the biogeochemistry and ecology of Arctic seas (e.g., Forest et al., 2014; Grebmeier et al., 2015; Arrigo, 2015 and references therein). For example, earlier ice melt and longer open-water duration may lead to a shift to greater pelagic primary production driven by increases in light penetration (e.g., Pabi et al., 2008; Arrigo et al., 2008; Zhang et al., 2010). Evidence that some of these processes are already occurring includes deepening of the nutricline and chlorophyll maximum in the interior of the Canadian Basin over the past decade (e.g., McLaughlin and Carmack, 2010), and possibly the new observations of massive

* Corresponding author.
E-mail addresses: mgoni@coas.oregonstate.edu (M.A. Goñi), corvie@onid.orst.edu (E.R. Corvi), welchk@oregonstate.edu (K.A. Welch), buktenim@onid.oregonstate.edu (M. Buktenica), lebonk@uw.edu (K. Lebon), Yvan.Alleau@oregonstate.edu (Y. Alleau), ljuranek@coas.oregonstate.edu (L.W. Juranek).

https://doi.org/10.1016/j.marchem.2019.03.010
Received 7 September 2018; Received in revised form 15 January 2019; Accepted 14 March 2019
Available online 19 March 2019
0304-4203/

blooms under first-year ice on the Chukchi Sea shelf (e.g., Arrigo et al., 2012, 2014; Balch et al., 2014). On the other hand, increased inputs of melt water (and river runoff) are expected to enhance stratification in the euphotic zone and can lead to the depletion of nutrients in surface waters during the latter part of the growing season (e.g., Yamamoto-Kawai et al., 2009; Jackson et al., 2011). Thus, while earlier melt may result in a change in timing of peak production (i.e. a shift towards earlier production), it is unclear how annually-integrated primary productivity will increase with potential limits imposed by the availability of nutrients.

The prolonged periods of open water over extensive sections of the Arctic during the summer and early fall season can lead to wind-driven mixing and upwelling that could supply nutrients to otherwise highly stratified, nutrient-poor surface waters (e.g., Pickart et al., 2009, 2011, 2013a). Modeling efforts, such as those of Zhang et al. (2010), and recent observational studies such as those of Ardyna et al. (2014) suggest that these processes could force a shift of pelagic ecosystems towards "sub-Arctic"-like conditions and the development of fall plankton blooms. Such shifts in the timing, magnitude and mode (ice vs. pelagic algae) of production have the potential to fundamentally affect key ecological processes by creating mismatches between food availability and energy requirements for higher trophic levels in the later season (e.g., Grebmeier et al., 2015, 2006; Forest et al., 2011; Moline et al., 2008).

In view of the rapid and unprecedented changes underway in the Arctic, there is a critical need for observations at spatial and temporal scales sufficient to capture the complexity of the system and help inform models and predictions of future trends (e.g., Anderson and Macdonald, 2015). In addition, the development of remote sensing capabilities, either through satellites (e.g., Chaves et al., 2015; Behrenfeld et al., 2017) or buoys, drifters, and gliders (e.g., Baumgartner et al., 2014; Hauri et al., 2018), requires high quality in-situ data to develop appropriate regional algorithms to interpret sensor outputs. In that context, several past and on-going initiatives, such as SBI and ICESCAPE, have developed rich observational data sets on biogeochemical and ecological conditions in regions such as the Chukchi Sea (e.g., Grebmeier et al., 2006, 2009; Arrigo, 2015). However, because of the rapid climate-driven changes in polar seas, questions still remain regarding processes occurring during the increasingly prolonged and geographically expansive late summer and fall open-water season. This is especially significant because the conditions of strong stratification and nutrient-limitation characteristic of this period may be impacted by advection, mixing and upwelling events (e.g., Danielson et al., 2014; Danielson et al., 2017; Pickart et al., 2013b; Weingartner et al., 2017).

Given the need for high-resolution observations during the late open-water season, we present over a thousand individual measurements of particulate organic matter concentrations and compositions (i.e. carbon:nitrogen ratios) from surface waters of the northern Bering Sea and Chukchi Shelf collected during four separate years. This extensive data set was collected using the surface underway systems of three different research vessels and a semi-automated filtration system that allowed sample collection at high frequency. In this paper we evaluate the application of this technique to Arctic waters, compare and contrast these observations to previous studies and evaluate the concentration and provenance of particulate of organic matter in different water masses from the region. Our findings indicate that the distributions of particulate organic matter along the western Arctic shelf reflect patterns of wind forcing and physical circulation, with regions of localized high standing stocks that are consistent with spatially and temporarily variable primary productivity during the late open-water season.

2. Study area

The northern Bering Sea and Chukchi Sea region is characterized by a broad and shallow shelf that has been the subject of multiple oceanographic studies (e.g., Coachman et al., 1975; Weingartner et al., 2005; Woodgate et al., 2015; Danielson et al., 2014; Danielson et al., 2017 and references therein). Briefly, the circulation over the Chukchi Sea shelf is to a large extent determined by the input of Pacific Ocean waters through Bering Strait, which include Anadyr Water, Bering Shelf Water and Alaska Coastal Water (ACW) (Fig. 1). The inflow through the Bering Strait is primarily forced by differences in sea-level between the Pacific and Arctic oceans (e.g., Stigebrandt, 1984) with local and regional forcings such as winds, heat exchange, ice melt/formation and river runoff, affecting the properties of these different water masses. Large seasonal and inter-annual contrasts in water mass inputs, as well as the modifications that occur during their transit through the Chukchi Shelf, have considerable impacts on the biogeochemistry of the region and the export of carbon and nutrients to the Arctic Ocean.

Once Pacific Ocean waters enter the Chukchi Sea, the inflow from the Bering Sea bifurcates into two bathymetrically controlled paths. One path moves water down Herald Canyon, located to the west of Herald Shoal, and the Central Channel, located between Herald Shoal and Hannah Shoal, and the other represents a buoyant, shoreline-constrained current (i.e., ACW). These flows deliver heat, freshwater, nutrients and organic matter to the Chukchi Sea impacting its ice, pelagic and benthic ecosystems (e.g., Arrigo et al., 2014; Grebmeier et al., 2015 and references therein). Anadyr Water tends to be highest in nutrients (e.g., $NO_3^- > 25\,\mu M$), with Bering Shelf Water and Alaska Coastal Water masses typically displaying moderate ($NO_3^- \sim 15\,\mu M$) and low ($NO_3^- < 10\,\mu M$) nutrient concentrations, respectively (e.g., Arrigo et al., 2014). These water masses undergo significant seasonal variations due to processes such as sea ice formation/melting, cooling/heating, mixing with river sources and biological productivity. For example, during winter the water column throughout much of the Chukchi Sea shelf undergoes complete vertical mixing due to sea ice formation and brine rejection. In the spring and early summer, as snow melts and sea ice thins, light penetration increases and the stratification of nutrient replete surface waters starts to develop, leading to large under-ice phytoplankton blooms. Much of this early production is efficiently exported to the benthos, decreasing nutrient concentrations in surface waters which become increasingly stratified as sea ice melt continues. By late summer, highly stratified conditions prevail over much of the Chukchi Shelf and surface waters are highly depleted in nutrients relative to deeper waters below the pycnocline. These conditions were encountered during the late summer and early fall cruises that were the focus of this project.

The strong and highly dynamic physical and biogeochemical oceanographic processes in the northern Bering and Chukchi Seas result in complex and highly variable surface expressions, such as particle distributions captured by NASA's MODIS imagery (Fig. 1 insert). This image clearly illustrates the complex interactions of currents, bathymetry, shoreline features and biologic responses that lead to multiple particle-rich plumes and filaments throughout the study area. Such complex surface expressions are challenging to study via conventional means of water sampling (e.g., CTD casts) but instead lend themselves to the high frequency sampling approaches described in this paper. While detailed examination of satellite measurements from the study region is beyond the scope of this work, this image provides a useful reference point from which to examine the surface POM distributions presented here.

3. Samples & cruises

The samples and data presented in this paper were collected during four separate cruises aboard three different research vessels, including United States Coast Guard Cutter (USCGC) Healy, National Oceanographic and Atmospheric Administration (NOAA) Research Vessel Ronald H. Brown and University-National Oceanographic Laboratory System (UNOLS) Research Vessel Sikuliaq, operated by

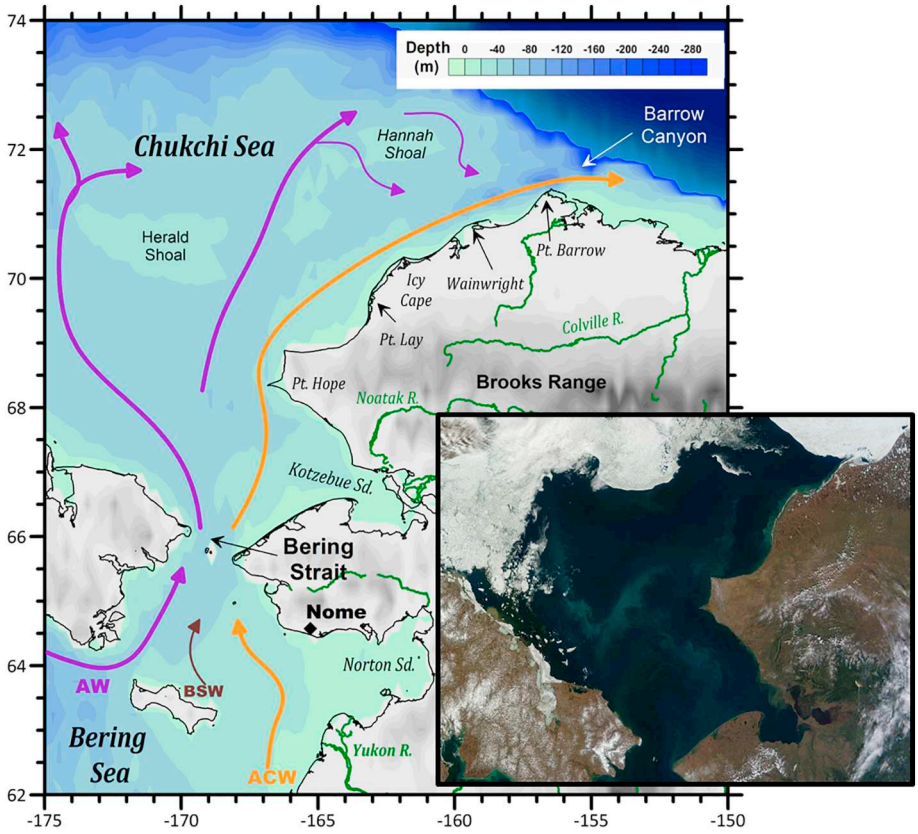

Fig. 1. Map of the study area showing the coastlines, bathymetry and general physical oceanographic circulation along the northern Bergin Sea and Chukchi Shelf (after Danielson et al., 2014). The three Pacific water masses entering the Chukchi Sea through the Bering Strait include Anadyr Water (AW), Bering Shelf Water (BSW) and Alaska Coastal Water (ACW) (e.g., Coachman et al., 1975; Danielson et al., 2017b). The insert in the figure represents a true color image of the Chukchi Sea in June 17, 2015 from the Moderate Resolution Imaging Spectroradiometer (MODIS) aboard NASA's Terra satellite (https://modis.gsfc.nasa.gov/gallery/images/image07012015_250m.jpg). (For interpretation of the references to color in this figure legend, the reader is referred to the web version of this article.)

University of Alaska-Fairbanks. The USCGC Healy cruise (HLY1203) sailed from Dutch Harbor to Dutch Harbor (AK) from October 5 to 25, 2012. The Ronald H. Brown cruise (RB1505) sailed from Kodiak (AK) to Dutch Harbor (AK) from August 6 to September 4, 2015. The RV Sikuliaq cruise in 2016 included a transit leg (SKQ201611T) from Seward (AK) to Nome (AK) from August 26 to 31, 2016 and a science leg (SKQ201612S) from Nome to Nome from September 3 to 25, 2016. In 2017, the RV Sikuliaq cruise included a transit leg (SKQ201711T) that sailed from Seward to Nome from August 1 to August 5, 2017 and a science leg (SQK201712S) from August 7 to 21, 2017. For the two Sikuliaq cruises, we have combined the data from each transit and science legs and will refer to those data sets as SKQ2016 and SKQ2017, respectively. All surface underway data (date and time, latitude, longitude, salinity, temperature, POC and PN concentrations) are available at the National Science Foundation's Arctic Data Center (https://arcticdata.io/) and published under https://doi.org/10.18739/A27W67535.

To provide insight into the wind forcing on surface waters of the region during these cruises, we downloaded wind data from NOAA's Barrow Met station (https://www.esrl.noaa.gov/gmd/obop/brw/) and plotted the east-west (U_{wind}) and north-south (V_{wind}) components of the wind speed vectors for the Aug-October months of 2012, 2015, 2016 and 2017 (Fig. 2). These data illustrate the highly variable winds that impact this northern most region of the Alaskan coastline. For example, during the first leg of the HLY1203 cruise, winds at Pt. Barrow were primarily from the northwest at moderate overall wind speeds (5–15 knots), with a strong shift to northeasterly winds in mid-October that resulted in overall wind speeds exceeding 25 knots, followed by variable southwest winds during the latter part of the cruise. In 2015, Pt. Barrow winds during the first part of the RB1505 cruise were predominantly easterly with variable magnitude. During the second part of RB1505, easterly winds increased to speeds exceeding 20 knots before switching in direction to westerly winds on Aug-24 as a strong storm front passed over the area. Overall wind speeds during this period approached 30 knots at Pt. Barrow and led to cessation of field operations aboard RV Ron Brown for a 48 h period. During the SKQ2016 cruise, Pt. Barrow experienced variable northerly winds of moderate magnitude (5–15 knots) during the first part of the cruise and a buildup of northwesterly winds during the second part that exceeded 20 knots on September 19. In 2017, Pt. Barrow winds during the SKQ2017 cruise period oscillated between southwesterly and northeasterly direction and moderate magnitude, with a relatively strong shift towards northeasterly winds on August 11 that lasted several days and resulted in overall wind speeds of almost 20 knots.

4. Methods

4.1. Sampling via surface underway systems

Most modern research vessels are fitted with surface underway systems that provide uncontaminated seawater to a variety of locations within the ship; including a sensor panel that at minimum records temperature and salinity, as well as taps for investigator-specific applications (e.g., Balch et al., 2014; Holser et al., 2011). The typical design of these scientific surface underway systems is illustrated in Fig. 3. Raw uncontaminated seawater is drawn via a sea chest, which is a recess cavity typically placed near the bow and below the water line (e.g., 4–8 m) that allows water to be pumped into the interior of the ship. Seachests vary in size (e.g., 0.1–1 m^3) but are designed to have unconstrained exchange of water from outside the hull with their openings typically protected by grates and/or baffles. Under normal underway conditions (e.g., ship speed and movement), this free exchange of water between the sea chest and the outside of the hull minimizes potential biases such as stagnation and particles settling inside the sea chest. A strainer basket with relative coarse mesh size (e.g., 1/16″ to 1/32″; 1.6 to 0.8 mm) is placed upstream of the pump to remove large particles and is cleaned on a regular basis to maintain normal operating pressures (e.g., 20 psi) and adequate flows for all

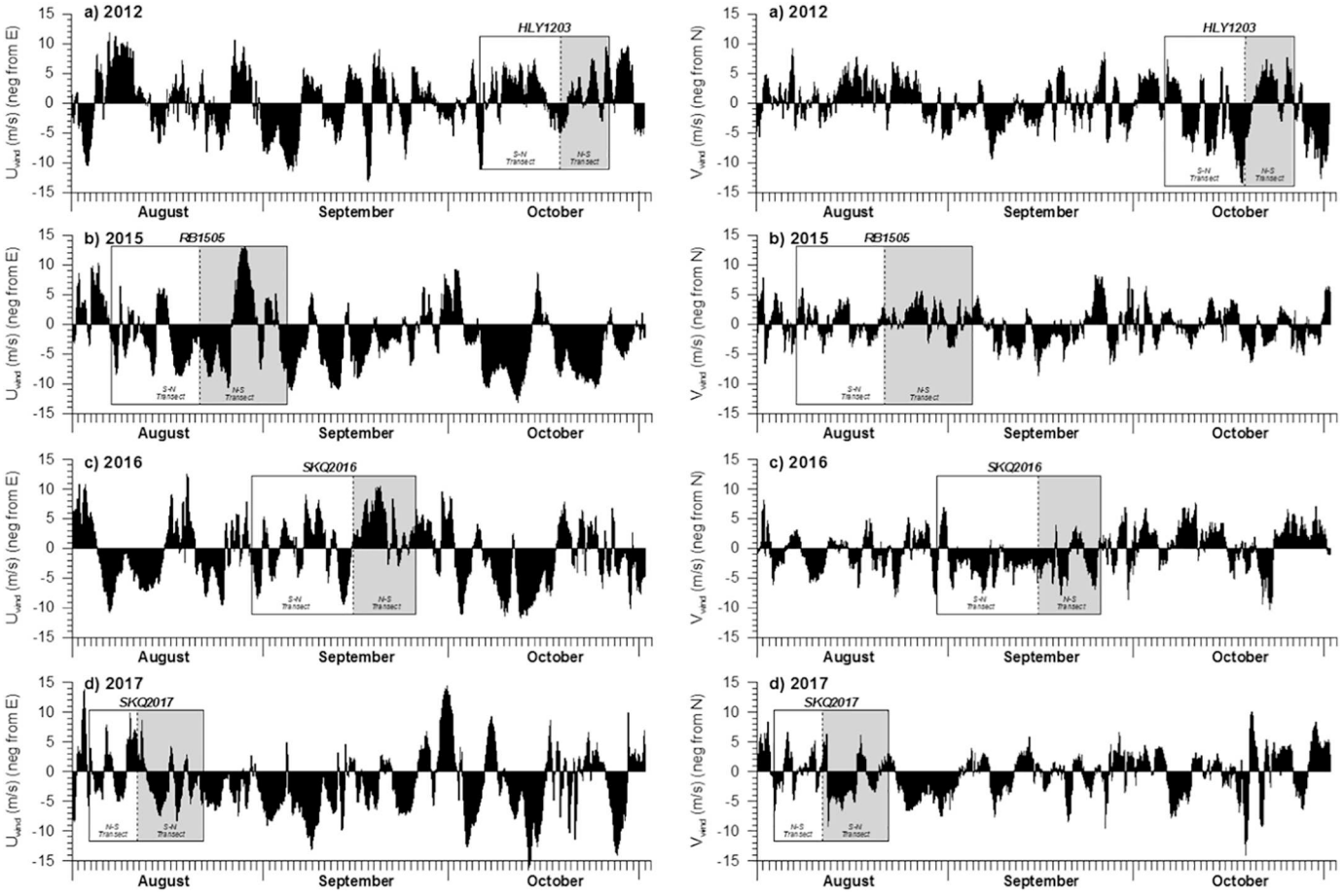

Fig. 2. Wind data, including east-west (U_{wind}) and north-south (V_{wind}) wind speed vectors, from Pt. Barrow Met station for the late summer/early fall period (August to October) in 2012, 2015, 2016 and 2017. The duration of each cruise is highlighted in each graph, including the S-N and N-S legs of each cruise. Upwelling-favorable conditions are characterized by easterly (negative U_{wind} values) and southerly (positive V_{wind} values) wind speeds, whereas westerly and northerly wind speeds are consistent with downwelling-favorable conditions along the coastline between Icy Cape and Utiqiavik. Wind and meteorological data products are available at https://www.esrl.noaa.gov/gmd/obop/brw/.

sensors and outlets (typically several liters per minute). While the design of the surface underway systems has the potential to bias against larger-size phytoplankton cells and underestimate phytoplankton biomass (e.g., Cetinić et al., 2016), initial studies showed the concentrations and compositions of bulk suspended particles collected via surface underway systems are comparable to those using other techniques (e.g., CTD rosettes, in-situ pumps; Goñi et al., 2017; Holser et al., 2011).

Newer research vessels utilize CPVC or Teflon-lined stainless steel piping to bring water from the sea chest to locations within the ship's wet lab(s), including a return flow to the sea that can be regulated to maintain appropriate pressures and flows as different taps are opened and closed during cruise operations. Most research vessels have regular maintenance schedules for surface underway systems, which include flushing pipes with fresh water after each cruise and periodically using caustic agents, such as bleach, to remove biological materials (e.g. biofilms, organisms such as filter feeders) that can potentially affect the chemistry of the water being pumped through the system (e.g., Juranek et al., 2010). Typically, temperature readings are measured upstream (e.g. at sea chest) and downstream (e.g., wet lab) of the pumps to constrain heating associated with the high-pressure flow of water through the ship's pipes. In this paper we use the measurements from upstream the pumps as a measure of sea surface temperature. Sieves in the strainers are periodically cleaned to remove coarse particulate materials and facilitate unconstrained flow. Many vessels have dual strainers with switching valves that allow uninterrupted operations while one of them is being serviced.

Samples for this study were collected aboard three modern research vessels with well-maintained surface underway scientific systems: USCGC Healy, NOAA's RV Ron Brown and UNOLS' RV Sikuliaq. Aboard each of the vessels we had access to uncontaminated seawater and collected samples at specific times that allowed us to determine location (latitude and longitude) and seawater characteristics (temperature and salinity) from the ships' navigation and sensor panels. In three of the cruises we had a semi-automated filtration system (SAFS; Fig. 3), similar to that described by Holser et al. (2011), which was used to collect particulate organic matter samples. We did not have the system available during the 2015 cruise aboard the RV Brown so we used manual vacuum filtration (e.g., Goni et al., 2003) of surface underway water to collect particulate samples. We used manual vacuum filtration during portions of the 2017 cruise when the SAFS unit was not available due to technical issues.

4.2. Semi-automated filtration of POM samples

The SAFS is designed to be connected directly to one of the taps in the ship's surface underway system and uses the flow and pressure in the line to push water through filters in order to collect particles. Our current SAFS model (Fig. 4) is similar to earlier designs (Holser et al., 2011) with the main differences being the diameter of tubing used and the software used to control the system and record flow/time data. Our filtration procedure has been described previously (Holser et al., 2011) but a detailed description is provided here. Surface underway water

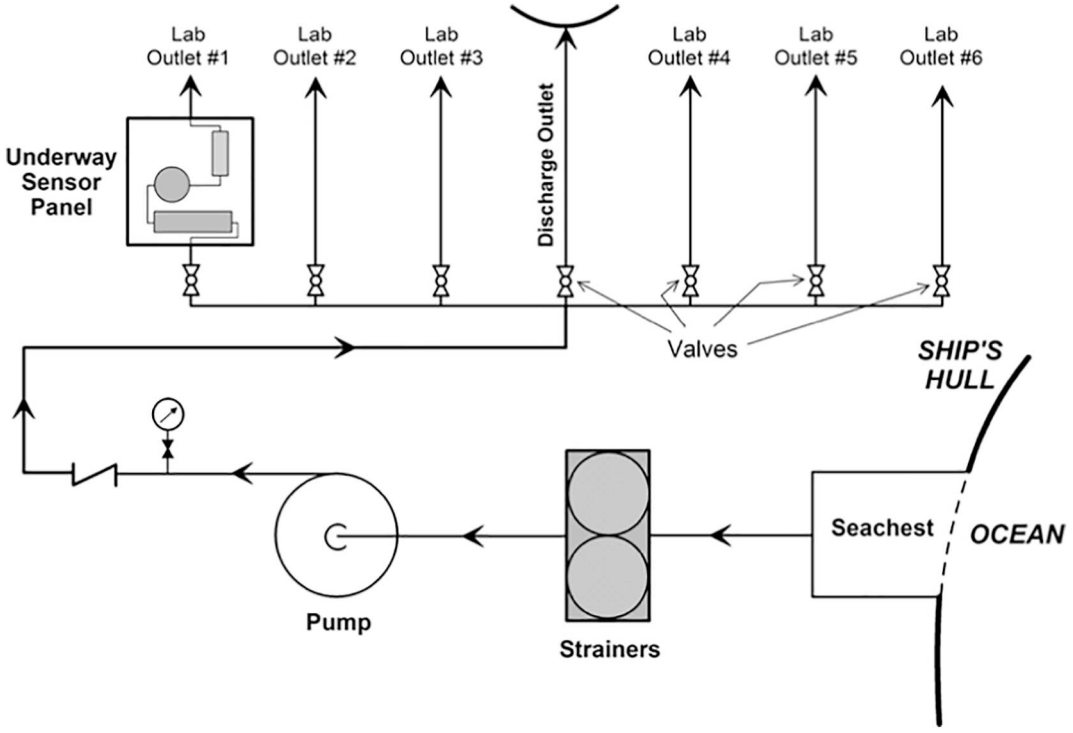

Fig. 3. Schematic of a typical surface underway system in modern research vessels.

was connected to the SAFS through a manual flow-control valve via opaque polyethylene tubing (3/16″OD × 1/4″" ID; McMaster-Carr). A fly wheel flow meter (Model# 101 Flo-Sen by McMillan Co.) was placed in-line and connected to a laptop computer via a NI-DAQ USB-6002 data acquisition system to measure and record flows during the filtration stage. The flow meter model has a range of 0–100 ml/min, so the flow control valve was adjusted to provide flow within this range. A switching valve with 8 ports (Model# CC4512-8148EUTA by Valco Instrument Company Inc.) was placed downstream from the flow meter and controlled by a Matlab program on the laptop. Under stand-by conditions, flow was directed to the 'waste' port, which was fitted with unobstructed tubing that drained into one of the ship's sinks and flowed back to sea. The 8-sample ports were fitted with tubing (1/4″ ID; McMaster-Carr), quick-turn sockets (Luer Lok fittings; McMaster-Carr) and in-line stainless steel 13-mm Swinney filter holders (Pall Life Sciences). The flow from these filters was directed to the same sink as the

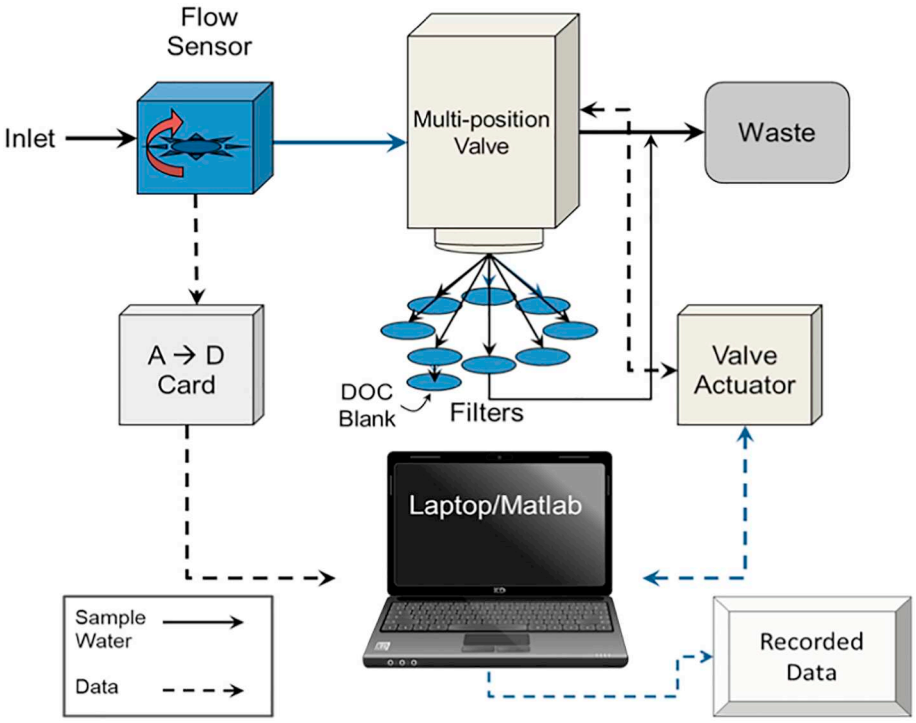

Fig. 4. Schematic of the semi-automated filtration system (SAFS).

'waste' flow. In each holder, we placed one pre-combusted (400 °C for 3 h) 13-mm glass fiber filter (Pall Life Sciences) supported by a stainless steel screen and locked into place with a Teflon o-ring that prevents leakage and results in a filtration area of 78.5 mm^2.

Once filters were fitted in each of the sample ports, the filtration program was started in Matlab to collect samples at selected intervals. The filtration program included code that allowed the operator to determine the period of time between filtrations, as well as the duration and/or volume of water collected through each filter. Under typical conditions, the system was programmed to collect a filter sample every 20 min during a 4 min interval, resulting in a total filtered volume of roughly 300 ml of water given flows of ca. 80 ml/min. Note that the flow rates through the filter, which were monitored continuously during the filtration process, decreased steadily as particles clog the filter and impede flow, potentially altering the particle retention characteristics of the filter membrane. For this reason, our filtration program included a minimum flow threshold (typically 20 ml/min) below which the filtration process was stopped.

Using the filtration settings described above, we were able to collect 8 samples every ca. 3 h. However, depending on navigation conditions and overall concentrations of POM in surface waters, we altered the filtration program to adjust the overall spatial resolution and the volume of water passed through each filter. Once the filtration run was completed, the filter housings were removed from the SAFS, opened, and each individual filter folded into pre-cleaned silver capsules (5 × 9 mm; Costech), which were placed into sample trays that were frozen until CN analyses. Each sample was assigned a specific time stamp (start-end of filtration process) that coincided with the ship's clock and allowed us to retrieve location and oceanographic data for each sample, as well as determine an overall filtration volume, which was used to calculate particulate nitrogen and carbon concentrations once their contents were determined. During normal operations, we stacked two filter holders at specific positions in order to collect both particles from a sample using the first filter as well as measure blanks associated with dissolved organic matter sorption as filtered water goes through the second filter (see below). The filter holders stack easily because of their Luer-Lok fittings.

4.3. Carbon and nitrogen measurements

Carbon and nitrogen analyses were conducted using high temperature combustion/reduction according to Goni et al. (2006). Because filters were already placed in silver boats, we were able to put them directly into Teflon trays and exposed them to concentrated hydrochloric acid fumes to remove carbonates. This step was typically done over a 24 h period after which samples were dried in an oven (60 °C) and then placed into tin capsules (5 × 9 mm; Costech) and folded carefully into round pellets that were placed in the CN analyzer auto-sampler (Zero-Blank Costech). Placing the silver capsules into tin capsules minimizes loss of sample during folding of the boats into spheres because the silver can become brittle after exposure to concentrated acid fumes.

Samples were run in two CN analyzers (NC2500 Thermoquest and ECS 4010 Costech) using the manufacturers' recommendations for carbon and nitrogen analyses (e.g., specified temperatures for combustion and reduction furnaces, O_2 loops/pressure, and the use of a water trap). Once placed in the auto-sampler, samples were purged with helium for several minutes, sealed and run sequentially until all of them were analyzed. Each individual sample analysis was 5 min long and allowed the chromatographic separation of N_2 and CO_2 gases for quantification. In each run of a full auto-sampler, we typically included 6 standards (e.g., cystine, atropine) with different and known amounts of carbon and nitrogen to develop distinct calibration curves for each run. The standards were dispersed among the samples so as to account for any possible variations in combustion efficiency within each run. We also included 2 silver/tin boats that were acidified along with the samples to evaluate procedural blanks. All filters (i.e. DOC-blanks and samples) were treated the same and we used the DOC blanks throughout each cruise to correct each individual sample (see below).

In our work, we favor the use of the 13-mm filters as opposed to the 25-mm filters used by other investigators because the smaller filters have lower thermal mass, which maximizes combustion efficiency during the high temperature combustion process, and smaller surface area, which results in lower blanks associated with DOC-sorption. The smaller diameter filters also fit nicely in the 5 × 9 mm silver and tin capsules, allowing us to use the 50-position carrousel in the Costech zero-blank autosampler. The larger 25-mm filters are more challenging to fold into capsules and because of their larger size require the use of the 30-position carousel, which limits the number of samples that can be analyzed per run, especially since we still include several calibration standards during each run. Complete combustion of these larger filters is also more challenging to achieve, typically requiring larger volume oxygen injections that shorten the life of the reduction column. In our opinion, although the smaller filters require a little more care to remove and fold, their benefits in terms of sample throughput and ease of operation are significant.

5. Results

5.1. High-resolution POM analyses and blank determinations

Using the SAFS in combination with a research vessel's surface underway system, it is possible to collect high resolution data sets of particulate organic matter (POM) distributions in surface waters along the ship's navigational path. One key issue that needs to be evaluated when performing this type of filtration procedure is to determine how much of the carbon (and nitrogen) within a specific filter sample is due to POM and how much reflects the sorption of dissolved organic matter (DOM) into individual filter matrices (e.g., Moran et al., 1999; Gardner et al., 2003). Most researchers approach the determination of DOM-sorption by running particle-free, filtered water over a blank filter and using the data from those filter-blanks to subtract the signal from filter-samples. With manual filtration, time and personnel constraints typically limit the number of samples for which DOM-blanks are determined, often resulting in data from a few selected samples used to correct whole data sets (e.g., Holser et al., 2011). This can be an issue when sampling different water masses over different periods and in different volumes, all factors which can affect the fraction of DOM sorbed in individual filters. The SAFS design allows for relative ease in determining DOM-sorption as it simply requires adding a second filter housing downstream for the one collecting the sample. One limiting issue with this approach is that the number of analyses basically doubles if every sample has its own DOM-sorption blank, which can become significant in terms of analytical costs when hundreds of samples are collected during individual cruises. With these constraints in mind, our normal mode of operations was to collect one DOM-blank per 8-samples, which under normal sample frequency (15 to 30 min) translated into a DOM-sorption determination every 2 to 4 h. Under normal cruising speeds (5–10 knots), this frequency meant DOM-blanks every 10 to 40 nautical miles. However, the flexibility of the SAFS allows adjustments to be made in order to improve spatial coverage if needed.

One example of how DOM-sorption blank data were collected and applied is provided in Fig. 5. The map in this figure illustrates the sampling coverage for POM determination using the SAFS during the HLY1203 cruise from Dutch Harbor (AK) to eastern Beaufort Sea and back in October 2012. The red and blue dots represent samples collected during the outgoing and returning legs of the cruise, with specific dates and locations identified. The insert graphs include DOC-sorption blank data, in units of μg carbon in blank filter per ml of water filtered, and the sample to blank signal ratio for each individual filtration where both sample and DOC-blank filters were determined. A total of 670 POM samples were collected during the 20-day cruise, with 84 of those

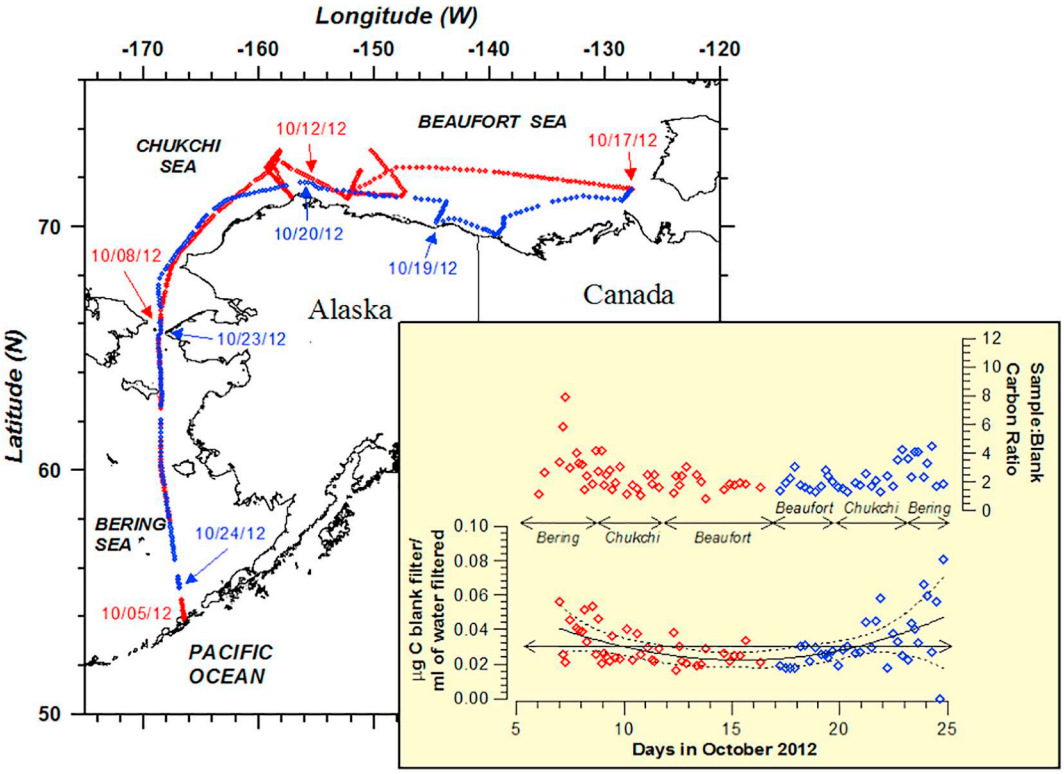

Fig. 5. Map showing sample distribution during the HLY1203 cruise with the insert showing the amount of carbon in filtered seawater blanks as a function of days of the cruise and the ratio of carbon measured in samples relative to their respective blanks. The polynomial fit of µg of C per ml filtered data is shown along with the 95% confidence intervals (µg C/ml = 0.08053–0.007155 X + 0.0001947 × ^{2} + 1.575 × 10^{-6} × ^{3}; where X = days in Octobers 2012). (For interpretation of the references to color in this figure legend, the reader is referred to the web version of this article.)

samples having DOM-sorption blank determination (ca. 13% of samples) including coverage along the Bering, Chukchi and Beaufort seas during both legs of the cruise. Note that there are some gaps in coverage that were associated with periods of time (hours to a couple of days) when the ship was not moving while recovering and deploying moorings (a main objective of the cruise) and the SAFS system was not used. Volumes filtered ranged from 150 to 400 ml per filter, with the larger volumes collected in regions of the Beaufort Sea where surface POM concentrations were lowest.

The amount of carbon (nitrogen data shown in electronic supplement) in DOM sorption blanks ranged from < 0.016 to 0.066 µg C/ml water filtered and an average of 0.031 ± 0.012 µg C/ml water filtered. There was a clear spatial trend indicating higher blanks in Bering Sea waters (and Chukchi Sea later in October) relative to their counterparts from the Chukchi and Beaufort Seas. The sample:blank carbon ratio in samples during the October 2012 cruise ranged from 1 to 8 with an average of 2.5. Samples from the Beaufort Sea had the lowest sample:blank ratios, an indication of the low POM concentrations in its surface waters at the time of the cruise. Given these data, our approach to correct for DOM-sorption was to fit the DOC-blank data (as well as the dissolved nitrogen; DN-blank data) with a third-order polynomial as a function of time (Days in October 2012). The fit and the 95% confidence intervals are shown in Fig. 5 and the actual function described in the caption. This empirical fit was used in combination with the volume filtered to calculate the amount of carbon and nitrogen associated with DOM sorption in each filtered sample and subtracted from the measured values. We chose to apply this correction, as opposed to other possibilities (see below), to capture the variability associated with water masses and provide conservative estimates of POM concentrations.

A contrasting example of DOM-sorption correction is provided in Fig. 6, which illustrates a similar application of SAFS but in this case for samples collected in late August and September of 2016 aboard the RV Sikuliaq. In this cruise, we had a transit leg north along the Bering Sea, a port-call in Nome and a return to Nome, which explains the locations of surface underway samples (total of 630) illustrated in the map and some of the time gaps in the DOM-sorption data. Other data gaps are due to the fact that operations during the cruise included the use of a towed vehicle for periods of time during which we shifted the connection of the SAFS from the surface underway system to the water being pumped into the ship's lab by the towed vehicle (e.g., Holser et al., 2011). Additionally, we encountered patchy sea ice cover in regions of the Chukchi shelf above 72 °N latitude in mid-September and had to use the bow thrusters extensively to push ice. Because the sea chest is located directly adjacent to the bow thrusters, we were concerned surface waters may be mixed by this process and typically minimized SAFS operations during those periods, explaining the lack of data during this part of the cruise.

As was the case for the 2012 cruise, we measured DOM-sorption blanks throughout the cruise when the surface underway-SAFS system was operating (n = 75, 12% of samples). Measured DOC blanks (as well as dissolved nitrogen blanks, data shown in electronic supplement) ranged from 0.004 to 0.088 µg C/ml water filtered (average of 0.020 ± 0.013). In contrast to the October 2012 cruise, for most of the 2016 cruise (September 5–27), DOC-sorption blanks fell within a fairly narrow margin (0.005–0.02 µg C/ml water filtered) with the exception of a few higher values measured during the transect across the Bering Sea in late August. Furthermore, sample to blank ratios were much higher (2 to > 10) in the 2016 cruise than in the 2012 cruise.

The trends described above were the result of lower DOM-sorption levels and higher POM standing stocks in waters of the study area during late August and September of 2016 than during October of 2012. Contrasts in the composition and concentration of DOM between periods and the overall abundance of particulate materials likely explain

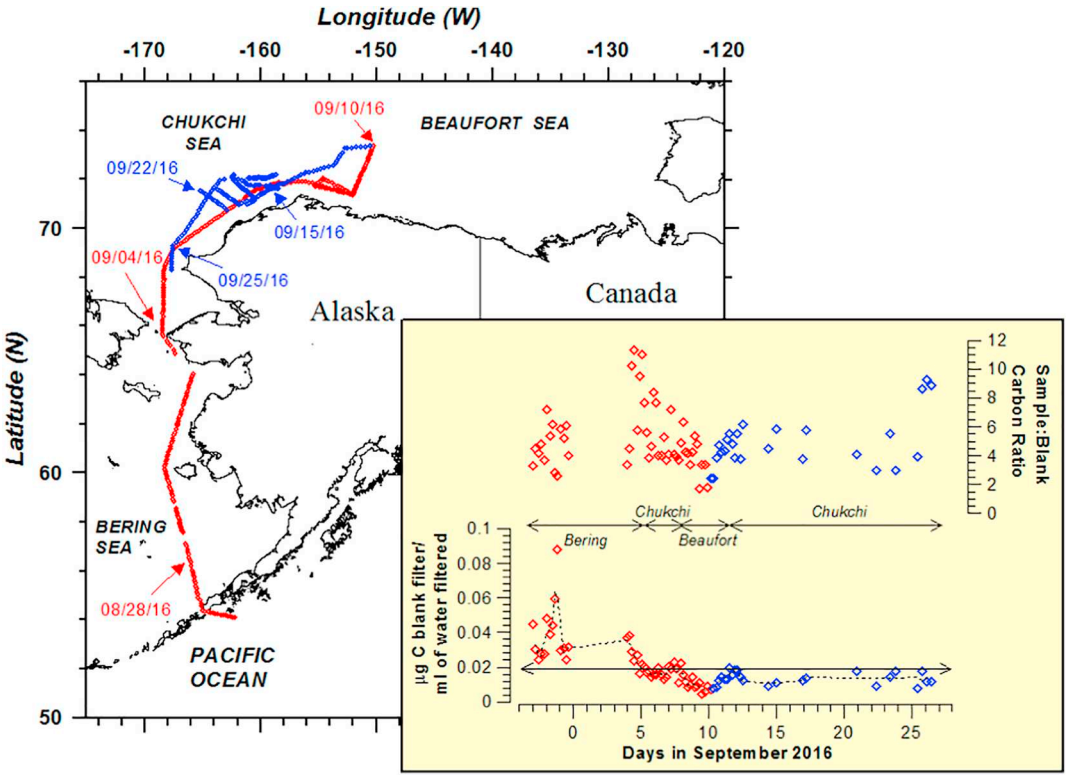

Fig. 6. Map showing sample distribution during the SKQ2016 cruise with the insert showing the amount of carbon in filtered seawater blanks as a function of days of the cruise, including the running average fit to the data, and the ratio of carbon measured in samples relative to their respective blanks. (For interpretation of the references to color in this figure legend, the reader is referred to the web version of this article.)

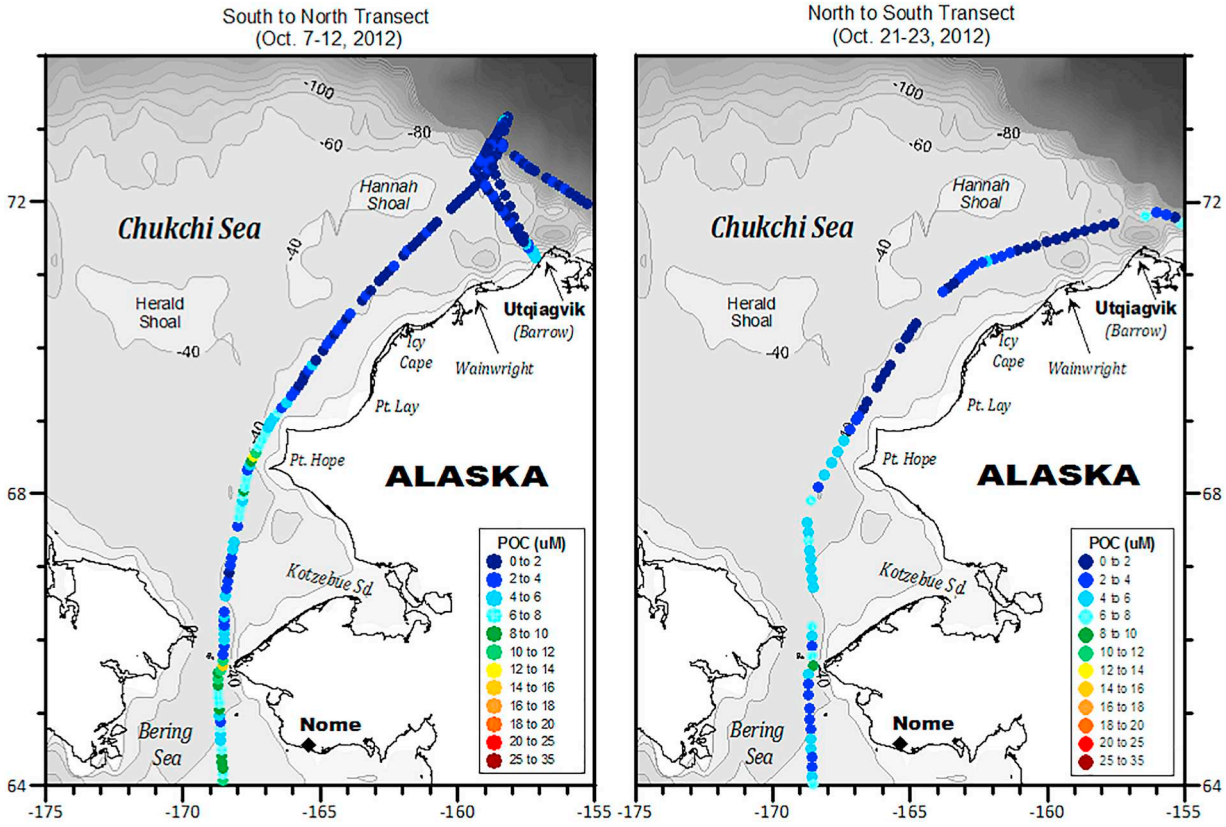

Fig. 7. Particulate organic carbon (POC) concentrations (micromoles per liter; µM) in surface waters from the northern Bering and Chukchi Sea collected via the surface underway system of USCGC Healy as part of the HLY1203 cruise during October 2012. (For interpretation of the references to color in this figure legend, the reader is referred to the web version of this article.)

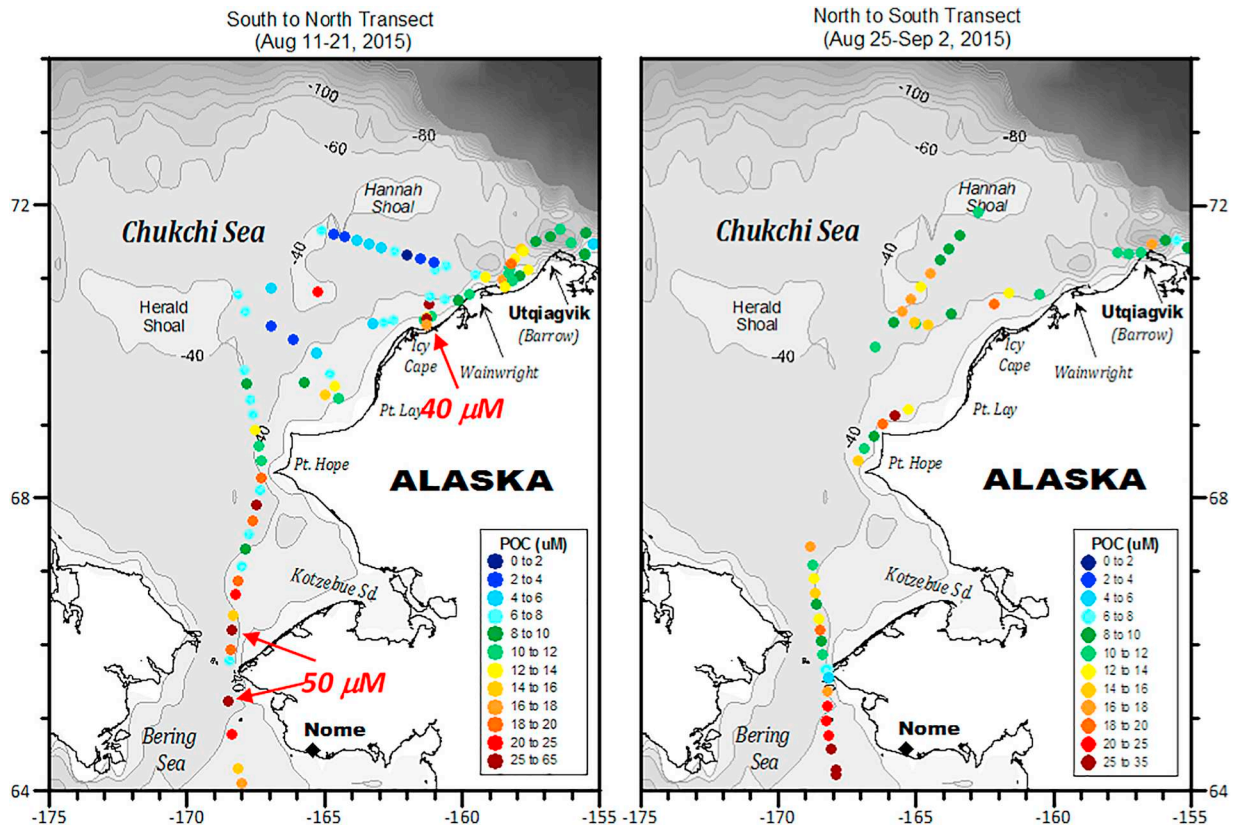

Fig. 8. Particulate organic carbon (POC) concentrations (micromoles per liter; μM) in surface waters from the northern Bering and Chukchi Sea collected via the surface underway system of NOAA RV Ron Brown as part of the RB1505 cruise during August 2015. (For interpretation of the references to color in this figure legend, the reader is referred to the web version of this article.)

these differences. In the case of the 2016 cruise, our DOM-sorption correction approach involved subtracting the running average DOC- and DN-sorption blank from the samples collected and having a distinct correction for the transit leg (Aug 28–31, 2016; Bering Sea) and the science leg (September 4–27, 2016; Chukchi and Beaufort Seas). We also used the running average approach to do the corrections for the August 2015 and 2017 cruises. Although more studies are needed to evaluate sorption dynamics of DOM in terms of seasonal and water mass contrasts, these results show the benefit of high resolution sampling and blank-determinations for studies of POM in surface waters.

5.2. Composition of surface waters of the Chukchi Sea

Because we have the most complete coverage and largest data sets for multiple years, the primary focus of this paper is the surface waters from the northern Bering and Chukchi Seas during the four cruises mentioned above (HLY1203, RB1505, SKQ2016 and SKQ2017). In order to present the data in a clearer fashion and illustrate spatial and temporal contrasts, we have divided each cruise into two transects (South to North and North to South) covering different periods and cruise paths. We present the data in map format using color dots to represent the ranges of values measured. In addition to POC concentrations (micromole per liter; μM) and the molar carbon:nitrogen ratios of POM ([C:N]), we present the average salinity and temperature (at sea chest) data corresponding to the filtration period of each sample. These data, along with the date/time, latitude, longitude and PN concentrations (μM) for all samples have been archived at NSF's Arctic Data Center and are available at https://doi.org/10.18739/A27W67535.

5.3. Particulate organic carbon concentrations

Overall, DOC-blank corrected POC concentrations in all four cruises ranged from ca. 0 to 35 μM, with several samples from cruises in August (RB1505 and SKQ2017) displaying higher values that ranged from 35 to > 60 μM. As a way to provide context for these ranges, previous applications of SAFS (e.g., Holser et al., 2011; Welch, 2015) have yielded POC concentrations > 50 μM in surface waters of the California Current during upwelling conditions, with values exceeding 100 μM in instances of sustained upwelling and high overall productivity. In contrast, less productive waters along the offshore regions of the California Current system were characterized by POC concentrations < 10 μM, with values lower than 3 μM in the most oligotrophic sections.

The ranges of POC concentrations measured along the northern Bering and Chukchi shelf are generally consistent with those previously measured by traditional methods (e.g., CTD casts and manual filtration) in surface waters from the region (0 to 80 μM; see regional compilations by Frigstad et al., 2014, Wyatt et al., 2013). However, there were important temporal and spatial differences. For example, POC concentrations during October 2012 were generally low, most samples displaying values that ranged from 0.2 to 8.0 μM (Fig. 7). Slightly elevated values (8–12 μM) were measured in a few samples located in the northern Bering Sea, as well as in the area adjacent to Bering Strait and Point Hope. The lowest POC concentrations were found along the northeast Chukchi Sea and in areas off the Chukchi slope in the western Beaufort Sea. In general, POC concentrations appeared to decrease later in the cruise, with lower values measured during the north-to-south transect in the latter part of October 2012 than during the earlier south-to-north transect. Data from the rest of the Beaufort Sea (see cruise track in Fig. 5) are available in the electronic supplement and were generally characterized by very low POC concentrations (0–2 μM). The main exceptions were a few samples from nearshore locations west of the Mackenzie River delta and from the Amundsen Gulf, where higher POC concentrations (4–12 μM) were measured.

The data from August 2015 (Fig. 8) were less numerous because

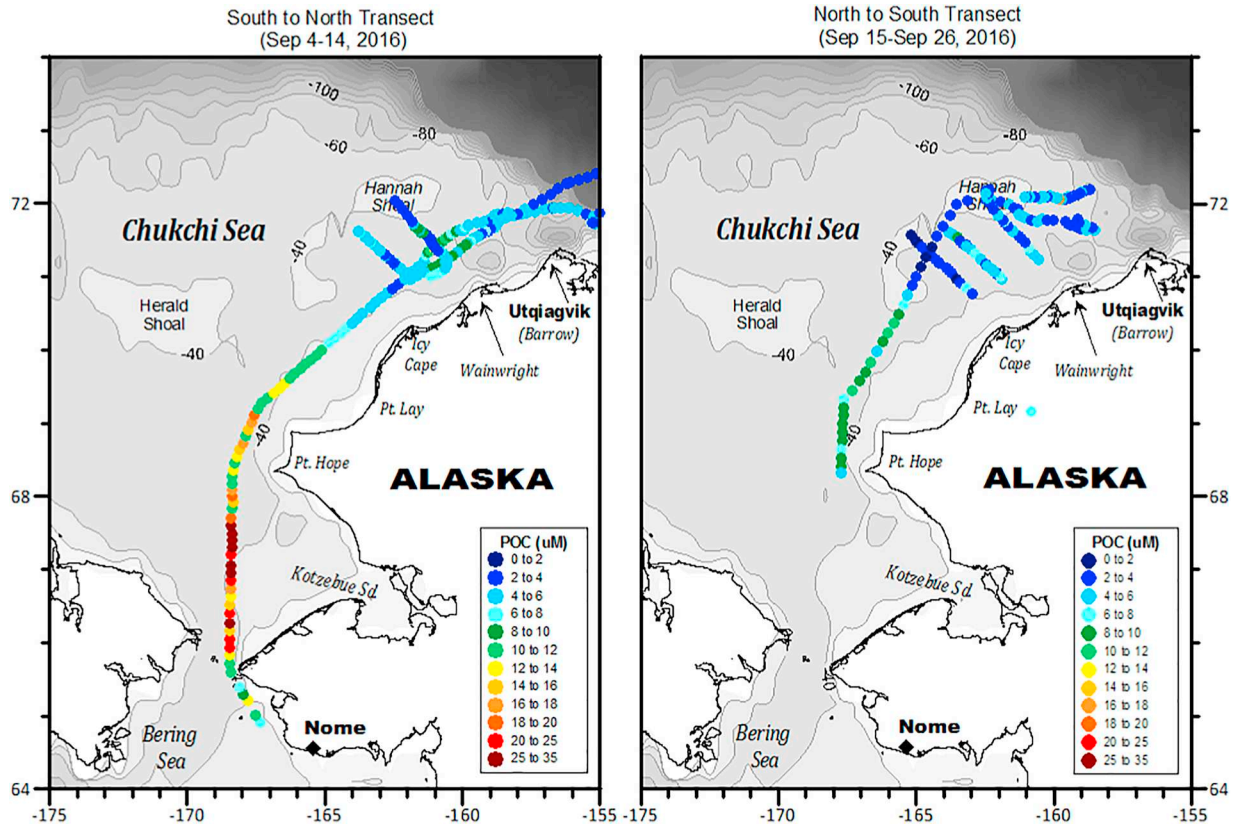

Fig. 9. Particulate organic carbon (POC) concentrations (micromoles per liter; μM) in surface waters from the northern Bering and Chukchi Sea collected via the surface underway system of UNOLS RV Sikuliaq as part of the SKQ2016 cruise during September 2016. (For interpretation of the references to color in this figure legend, the reader is referred to the web version of this article.)

manual filtration was used during the RB1505 cruise. Nevertheless, several significant trends are worth pointing out. First, POC concentrations were markedly higher on this cruise compared to the HLY1203 cruise, ranging from 2 to over 50 μM. As was the case with the previous cruise, the highest POC values were measured in a few locations around Bering Strait and Pt. Hope, with high concentrations also measured in the nearshore region between Icy Cape and Wainwright. The lowest concentrations (ca. 2–8 μM) were measured in offshore regions along the central Chukchi Shelf but only during the early (south-to-north transect) part of the cruise. Generally higher POC concentrations were measured during the north-to-south transect later in cruise (Aug 25-Sep 2). Notably, a large storm occurred during August 28–30, 2015, which was characterized by high winds that shifted in direction abruptly as the storm passed over the region (see Fig. 2) and forced cessation of science operations for those days. The higher POC concentrations measured in the region between Herald and Hannah Shoals during the latter part of the cruise may be a response of mixing associated with this event (see salinity and temperature plots below). It is important to note that the cruise track in August 2015 included many nearshore locations that were not occupied during the HLY1203 cruise so that direct comparisons of these two (and other) periods are difficult without accounting for contrasts in water masses (see discussion).

POC concentrations during September 2016 (SKQ2016) showed clear spatial trends with relatively low values (ca. 0–8 μM) north of Icy Cape and considerably higher values (8–35 μM) in the southern region of the Chukchi Sea and northern Bering Sea (Fig. 9). The lowest concentrations were found around Hannah Shoal, a region where we encountered significant pack ice. Because of the challenges of navigating through the pack ice and the time constraints they represented, we did not occupy many stations north of Hannah Shoal. However, there were some sections south of Hannah Shoal with moderately elevated (8–12 μM) POC concentrations. Notably, because the timing of this cruise coincided with the aboriginal subsistence whaling season, we were unable to occupy stations within 30 nautical miles from shore along the coast from Pt. Hope to Utqiagvik. The highest POC values were measured during the early part of the cruise in the region between Bering Strait and Pt. Hope. Although technical issues prevented us from collecting samples on the last 24 h of the cruise (section between Pt. Hope to Nome), the data indicate lower overall POC concentrations during the latter part of September relative to earlier in the cruise.

Fig. 10 illustrates the distribution of POC concentrations during August of 2017 (SKQ2017), which ranged from < 2 to 65 μM. The lowest concentrations (2–6 μM) were measured off Wainwright and in the more offshore region around Hannah Shoal, whereas the highest POC concentration were measured in the southern Chukchi sea region, as was the case with other cruises. Similar to the August 2015 cruise, several samples exhibited elevated POC concentrations above 35 μM, which were primarily associated with locations adjacent to coastal features such as Pt. Hope and Bering Strait. In contrast to the cruise in September 2016, there were no access restrictions due to whaling activities so many of the samples collected during SKQ2017 were within 30 miles from shore, where we did measure relatively high POC values. We completed several transects offshore, but we were unable to collect surface underway samples simultaneously while completing CTD and/or towed vehicle transects. The data from those efforts will be presented in separate publications. Notably, we measured increases in POC concentrations along the coast between Icy Cape and Wainwright from values of 4 to 16 μM earlier in the cruise (Aug 8–9, 2017) to values from 16 to > 30 μM later on (Aug 21–22, 2017).

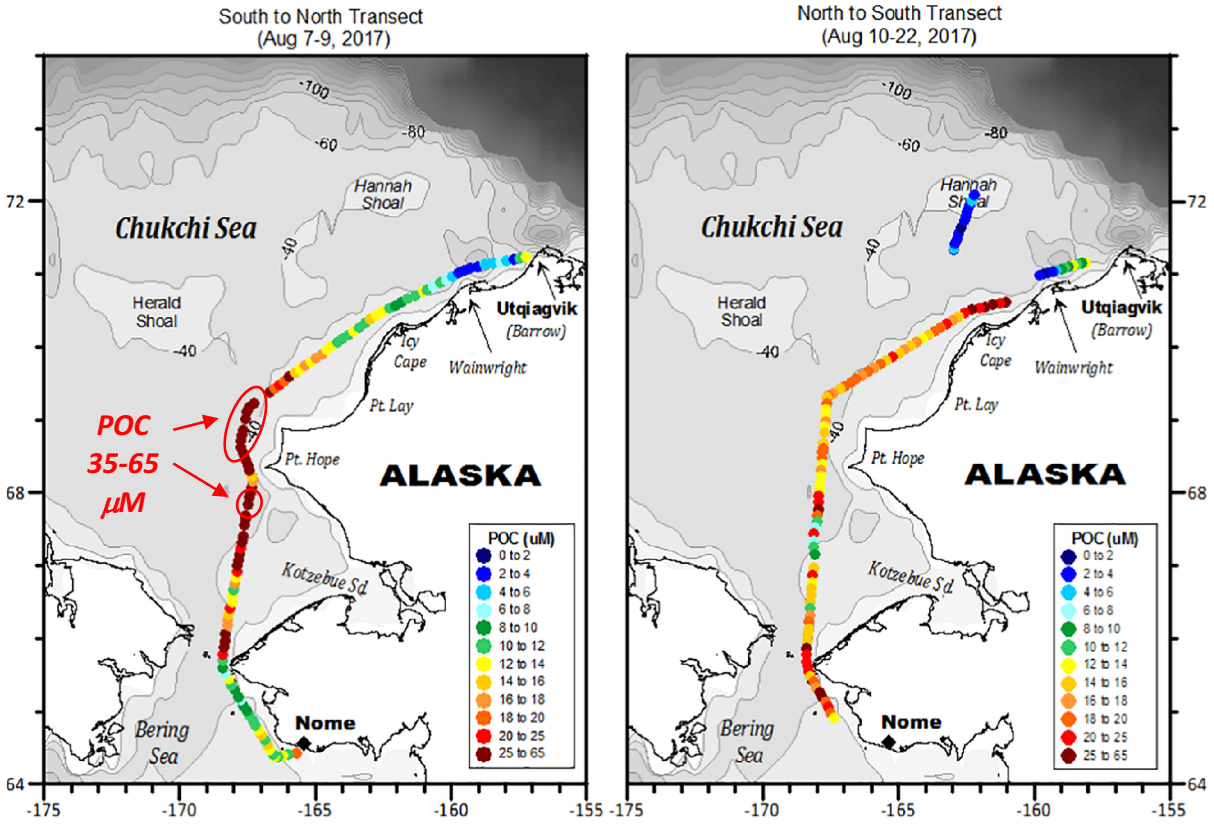

Fig. 10. Particulate organic carbon (POC) concentrations (micromoles per liter; µM) in surface waters from the northern Bering and Chukchi Sea collected via the surface underway system of UNOLS RV Sikuliaq as part of the SKQ2017 cruise during August 2017. (For interpretation of the references to color in this figure legend, the reader is referred to the web version of this article.)

5.4. POM carbon:nitrogen ratios

Particulate nitrogen (PN) concentrations ranged from 0 to 5 µM and displayed distributions that were similar to those of POC (see https://doi.org/10.18739/A27W67535) and resulted in molar [C:N] of particulate organic matter that ranged from 5 to 18 mol:mol (Fig. 11 a–d). The vast majority of the samples from the HLY1203 cruise were characterized by [C:N] ratios between 5 and 10, as was the case for samples collected during the RB1505 cruise. Most of the POM samples from the SKQ2016 and SKQ2017 cruises also displayed [C:N] values between 5 and 10 mol:mol, although in both cases several samples were characterized by significantly higher values (10–15). These latter samples coincided with some of the high POC regions between the Bering Strait and Pt. Hope., as well as selected nearshore locations. Overall, most POM samples from all four cruises exhibited [C:N] ratios that fell within the Redfield ([C:N] of 6.6) and Sterner ([C:N] of 8.3; Sterner et al., 2008; Frigstad et al., 2014) averages, with a small number of samples exhibiting values that deviated from this range.

5.5. Sea surface salinity and temperature compositions

As was mentioned previously, comparison of surface POM concentrations and compositions among different cruises and years is difficult because of the variability in water masses that characterizes the northern Bering and Chukchi Seas during summer and fall seasons (e.g., Danielson et al., 2017). For that reason, it is useful to examine the salinity and temperature of surface water samples collected via the surface underway system in order to characterize compositions of different water masses. Salinities throughout the study area during the four cruises ranged primarily from 24 to 34 with marked spatial and seasonal contrasts (Fig. 12 a–d). Salinities were uniformly high during the 2015 and 2017 August cruises, with most locations exhibiting salinities of 30–34. Lower salinities were observed during the September 2016 and October 2012 cruises, especially in regions north of Icy Cape and in the case of the HLY1203 cruise south of Pt. Hope, where salinities ranged primarily from 26 to 30. Overall, measured salinities were comparable to previous data from surface waters of this region collected during later summer and fall (e.g., Danielson et al., 2017).

Similar to salinity distributions, sea surface temperatures varied significantly throughout the study area among the four cruises, with most samples falling within the range of −1 to 12 °C (Fig. 13 a–d), which is similar to previously recorded surface temperatures in the region during later summer and fall (e.g., Danielson et al., 2017). Water temperatures were uniformly cold throughout the Northern Bering and Chukchi Seas in October 2012, with most measurements ranging between 0 and 4 °C. Subzero sea surface temperatures were measured south of Hannah Shoal during the latter part of the cruise, whereas the warmest temperatures (4–6 °C) were measured during the earlier cruise periods between Pt. Hope and Icy Cape and in the nearshore region off Utqiagvik. Relatively cold temperatures (−1 to 4 °C) also were measured north of Icy Cape during the September 2016, especially in the region around Hannah Shoal where we encountered broken sea ice. Unlike the October 2012 cruise, however, much warmer temperatures characterized the southern portion of the Chukchi Sea, with measurements between 8 and 12 °C throughout much of the region in early September 2016, and up to 14 °C south of Bering Strait. Lower temperatures (4 to 7 °C) were measured around the Pt. Hope region later in September 2016. Significantly warmer temperatures (6 to 12 °C) were measured throughout the study area during both 2015 and 2017 August cruises. This trend was especially noticeable north of Pt. Hope, where for example temperatures exceeded 10 °C during August 2017. The unusually warm conditions during this period included the very high

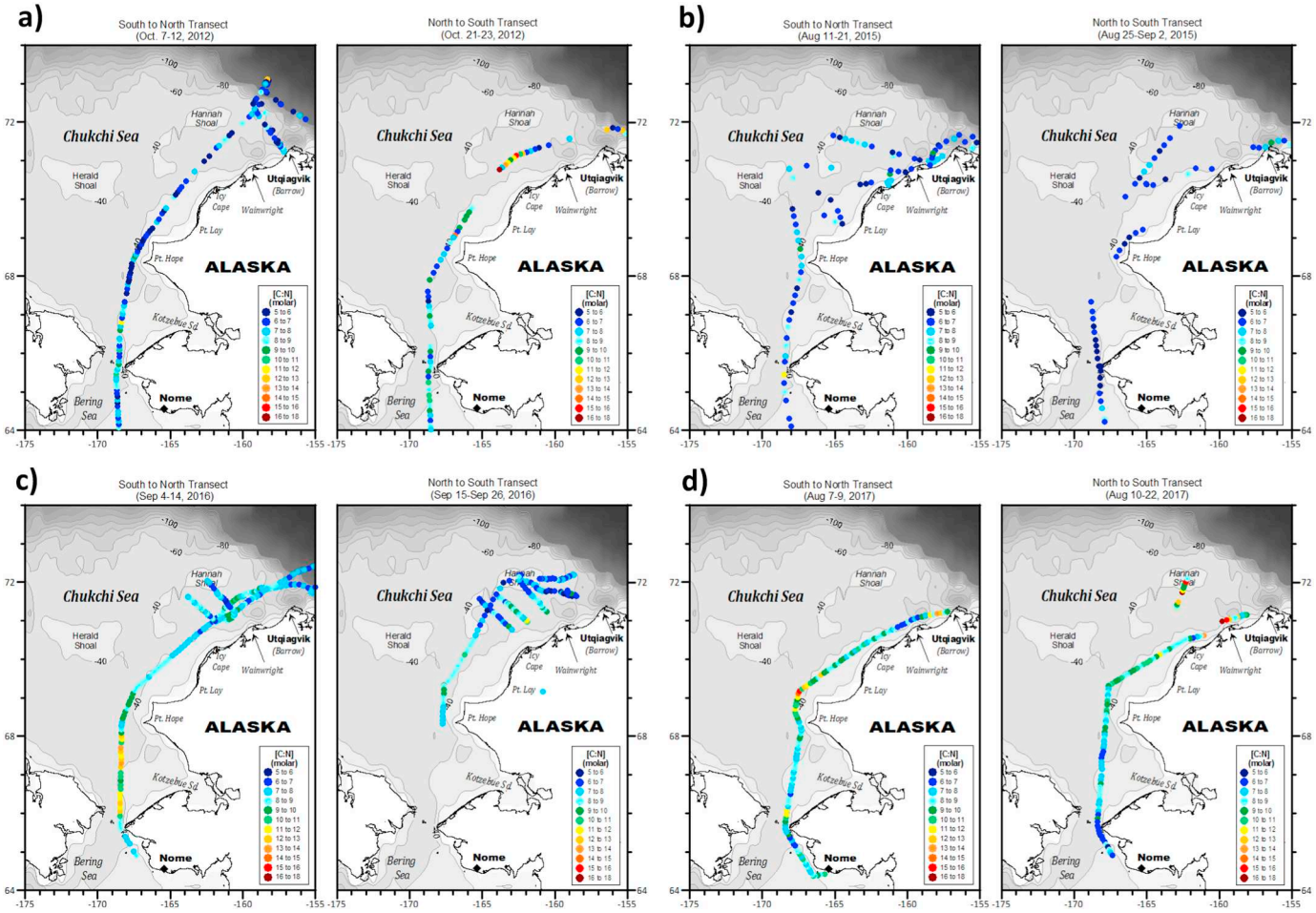

Fig. 11. Molar carbon to nitrogen ratios ([C:N]) of POM samples from the northern Bering and Chukchi Sea collected via surface underway systems during the following cruises: a) HLY1203, b) RB1505, c) SKQ2016 and d) SKQ2017. (For interpretation of the references to color in this figure legend, the reader is referred to the web version of this article.)

sea surface temperatures (15 °C) measured off Nome, which represent marked deviations from previous late summer-fall observations (e.g., Danielson et al., 2017). Several colder water fronts were evident along the cruise track in the southern Chukchi (e.g., offshore Kotzebue Sound), which coincided with salinity fronts and highlighted the complex surface water mass distributions in this region of the western Arctic (see Fig. 1 insert).

6. Discussion

6.1. Overall POM distributions

6.1.1. POC concentrations

The data sets presented above represent a significant increase in the number of observations available on the distribution of POM in surface waters from the Pacific Arctic. Based on the measurements illustrated in Figs. 7–10, it appears that POM standing stocks tend to be higher in the southern portion of the study area (64 to 69 °N of latitude) between Nome and Pt. Hope than along the northern section (69 to 74 °N of latitude) between Pt. Hope and north of Utqiagvik (Barrow). In Table 1 we summarize POC concentrations and [C:N] ratios of POM for these two geographical regions, showing averages, standard deviations and number of samples from the four different cruises and separate south-to-north and north-to-south transects (A and B, respectively). Overall, these data indicate POC concentrations tend to be higher earlier in the summer-fall season (e.g. August–September) than in the latter period (September–October).

Also summarized in Table 1 are data sets from selected previous studies of the region carried out by traditional CTD sampling (Yu et al., 2012; Chaves et al., 2015; Yamada et al., 2015; Arrigo et al., 2012, 2014, 2017), which show overall comparable ranges in concentration and composition to our surface underway measurements. The averages and standard deviations for previous data sets correspond to samples taken from the top 10 m of the water column and, as was the case with our data, we organized the data sets based on location (south or north of Pt. Hope) to facilitate comparisons. As it is evident from these regional averages, POC concentrations in early to mid-summer (June, July and August) tend to be higher than the averages later in the season (September–October). The data suggest a relatively prolonged productive season especially south of Pt. Hope, although given the complex circulation in this area, it is challenging to make more robust interpretations without investigating individual water mass compositions (see below).

Among the data sets north of Pt. Hope, the pre-bloom under ice data (POC ca. 5.5 μM) and under ice bloom conditions (POC > 40 μM) measured by Arrigo and co-workers in May–June and July (respectively) present interesting contrasts to the post-melt conditions we measured in August–October. From these data, it appears that as the seasons progress, POC concentrations increase during the under-ice spring bloom and then remain relatively low and stable for the rest of the summer-fall open water season. A more robust evaluation of conditions later during the melt season warrants evaluation of trends within specific water masses, which we attempt in the next section.

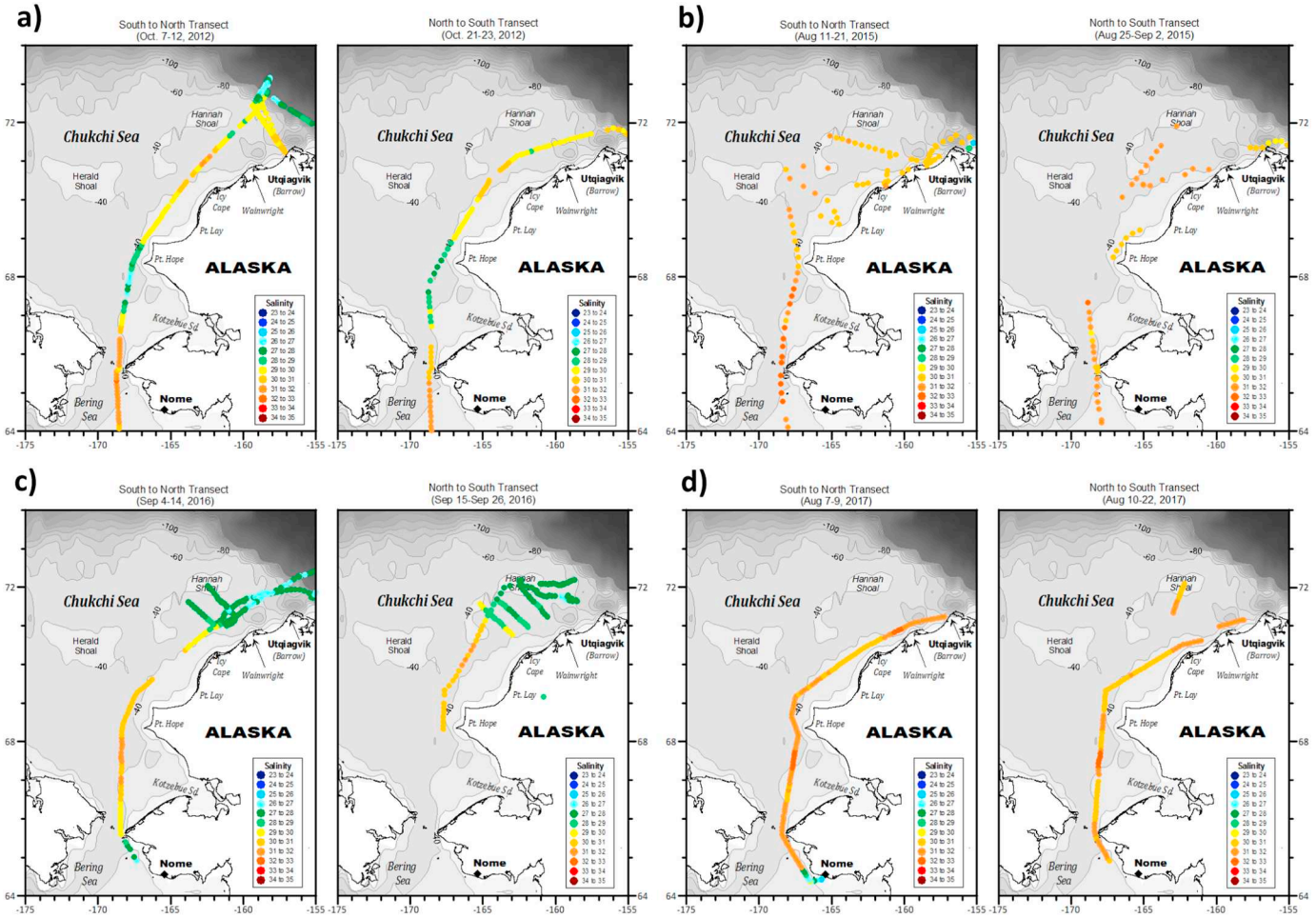

Fig. 12. Salinity of water samples from the northern Bering and Chukchi Sea collected via surface underway systems during the following cruises: a) HLY1203, b) RB1505, c) SKQ2016 and d) SKQ2017. (For interpretation of the references to color in this figure legend, the reader is referred to the web version of this article.)

6.1.2. *[C:N] compositions*

Based on the data in Table 1, it appears that for the most part [C:N] ratios do not display clear spatial or temporal differences, with most samples falling within the 6–8 mol:mol range characteristic of marine provenance (e.g., Redfield and Sterner ratios; Frigstad et al., 2014). Evaluation of the relationship between PN and POC (Fig. 14) reveals the data can be reasonably well described by a power relationship that is very similar to the one developed by Frigstad et al. (2014) based on a series of pan-Arctic data sets. Again, these results reinforce the point that the surface underway-SAFS system allows for representative high-resolution sampling of surface waters in Arctic seas.

Despite the overall similarities among our data sets, it is important to highlight some contrasts. For example, note that there are some cases in the HLY1203 data set where the number of POC and [C:N] measurements are different because of the fact that PN concentrations were so low in some of these samples as to not allow calculation of [C:N] ratios. Some samples from both south and north of Pt. Hope exhibit [C:N] ratios that are markedly higher than the 'normal' range of 6 to 8 (Table 1). For example the average [C:N] rations for the first leg of SKQ2016 (Sep 4–14, 2016) between 64 and 69 °N and those from the region north of Pt. Hope during the SKQ2017 legs (August 7–9, 2017 and Aug 10–22, 2017) all are markedly higher (9 to 10 mol:mol) than the Redfield and Sterner ratios. These higher ratios may reflect changes in phytoplankton physiological state, contrasts in freshness of material contributing to the POM and/or inputs from terrestrial sources (e.g., Arrigo et al., 2014; Frigstad et al., 2014). Note that among the previously published data sets for this region of the Arctic, those during the under-ice bloom also exhibit significantly higher [C:N] ratios (9.6 ± 4.1), consistent with the high levels of productivity and nitrate depletion in surface waters (Balch et al., 2014).

6.2. *Water mass distributions*

Although the spatially-grouped averages discussed above are helpful in interpreting the trends within the data sets of this and previous studies, it is clear that the complexity in the distribution of water masses hinders comparisons among different cruise periods. For that reason, it is helpful to investigate compositions of physically and chemically distinct water masses. Multiple studies have described the currents and water masses that typically characterize this region of the western Arctic (e.g., Weingartner et al., 2005; Danielson et al., 2014 and references therein). Briefly, waters entering the Chukchi Sea through the Bering Strait include Anadyr Water, Alaska Coastal Water (ACW) and Bering Shelf Water. The temperature and salinity characteristics of these Pacific-origin water masses are subject to significant changes during their transport along the Chukchi Shelf due to processes such as cooling-heating, sea-ice forming and melting, and river discharge (e.g., Woodgate et al., 2015; Woodgate et al., 2012). Thus, the literature often defines these modified water masses based on the temperature-salinity characteristics with names like, Bering Shelf Summer Water, Bering Shelf Winter Water, Chukchi Shelf Summer Water, Chukchi Shelf and Winter Water (e.g., Danielson et al., 2017 and references therein). For this study, we used the approach of Danielson et al. (2017b) and grouped Bering and Chukchi Shelf waters into

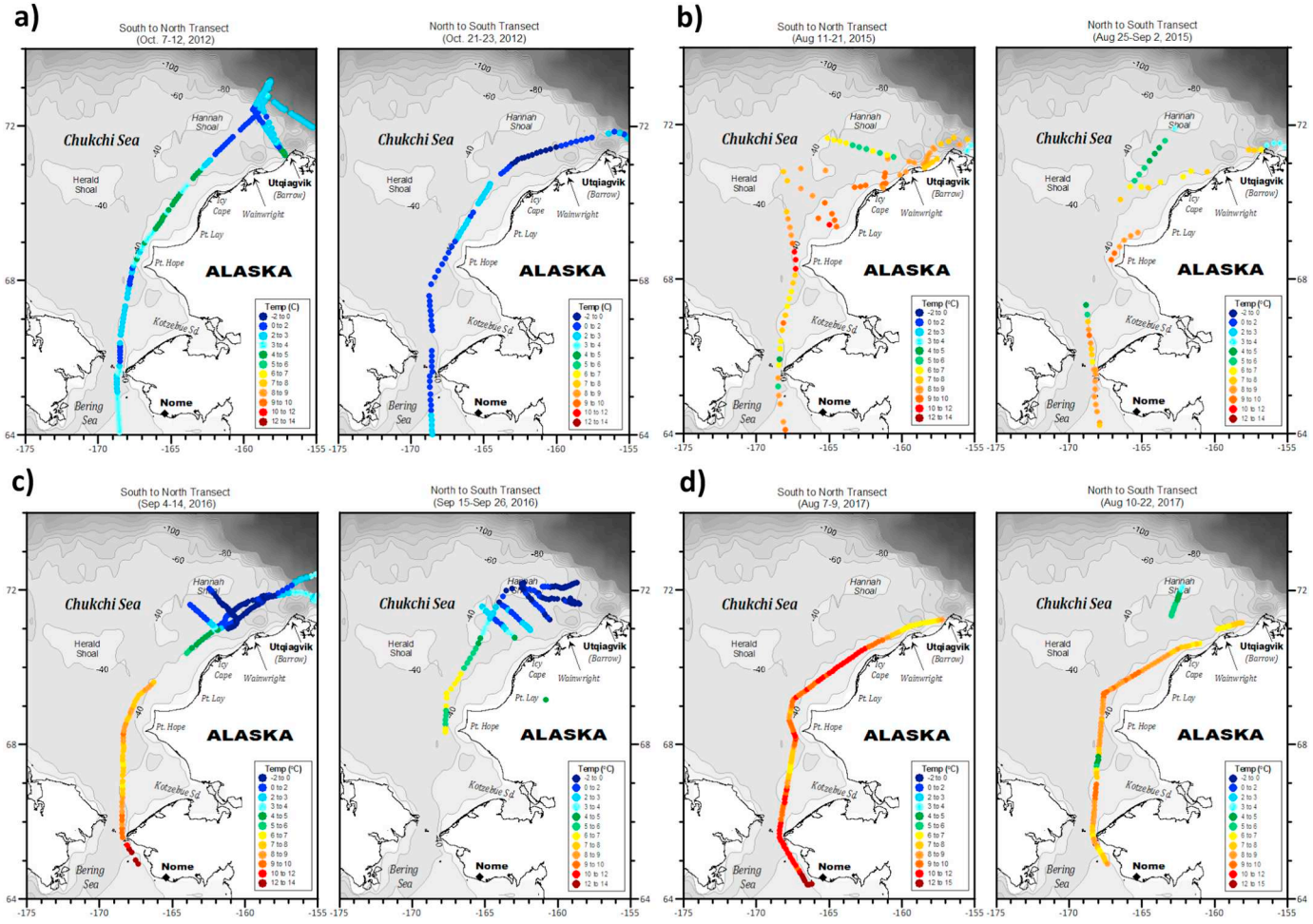

Fig. 13. Temperature data (measured at the sea chest) for water samples from the northern Bering and Chukchi Sea collected via surface underway systems during the following cruises: a) HLY1203, b) RB1505, c) SKQ2016 and d) SKQ2017. (For interpretation of the references to color in this figure legend, the reader is referred to the web version of this article.)

Bering-Chukchi Summer Water (BCSW) and Bering-Chukchi Winter Water (BCWW). Similar to Danielson and co-workers, we also considered sea ice Melt Water (MW) as another regional water mass.

Table 2 shows the temperature and salinity ranges for these water masses as defined by Danielson and co-workers, while Fig. 15 illustrates the composition of all the surface water samples collected as part of this study. Note that in this salinity-temperature diagram, we extended the ranges of ACW to include the significantly warmer and slightly saltier samples we measured in 2016 and 2017. This graph reveals that distinct water masses were encountered along the western Arctic shelf during the four different late summer-fall cruises. For example, during October 2012 (HLY1203), the vast majority of the surface POM samples were from two water masses; MW, which in some cases had lower salinities than the 25 range defined by Danielson et al. (2017b), and BCSW. In contrast, during the August 2015 (RB1505) cruise, filter samples collected via the surface underway system were primarily from ACW and BCSW, with only a few samples being from MW. Similar contrasts were seen between the two Sikuliaq cruises, with the one in September 2016 having a large number of samples from MW and fewer from BCSW and ACW. On the other hand, the August 2017 cruise (displayed samples that fell predominantly within the ranges of ACW, with only a few samples belonging to BCSW. As illustrated by the maps showed previously (Figs. 7–13), these differences among cruises are a function of both seasonal and interannual variability as well as the specific path of each cruises' ship track.

6.3. Water mass-specific POM distributions

Additional insights can be gained by examining the distribution of POM in the context of salinity vs. temperature plots (Fig. 16 a–d). In these graphs, we used different colors to represent the ranges in POC concentrations of individual samples from different water masses. Using these data, it is possible to examine in detail trends from specific water masses and hypothesize possible processes that may influence variability in compositions. However, an important caveat to keep in mind is that these observations represent surface expressions of oceanographic phenomena, including mixing of nutrients and organic matter and their biologic responses, in a region characterized by highly-stratified water columns and nutrient-poor surface waters (e.g., e.g., Arrigo et al., 2014; Danielson et al., 2017). While wind forcing data from Pt. Barrow met station provide information on possible wind-driven forcings (e.g., upwelling vs. downwelling favorable conditions, mixing), more detailed mechanistic explanations require observations throughout the water column, which are the subject of future papers with that focus.

In the case of MW, it is evident from the data in September 2016 (SKQ2016) and October 2012 (HLY1203) that this water mass was characterized by very low (< 6 μM) POC concentrations. The main exceptions were samples with higher POC values (6–12 μM) from locations between Hannah Shoal and Barrow Canyon in early September 2016 (Fig. 9) and directly off Pt. Hope in early October 2012 (Fig. 7). The elevated POC measurements in 2016 coincided with a period (Sep 10–15) of strong (ca. 20 knots) upwelling-favorable northeasterly winds

Table 1
Summary of particulate organic carbon (POC) concentration and particulate carbon:nitrogen ratio (C:N) data for surface waters (0–10 m) in the northern Bering Sea and Chukchi Sea region.

Cruise and period of study	POC (μM)				[C:N] (molar)				Citation	DOC correction
	Avg	±	Sdev	n	Avg	±	Sdev	n		
64–69 °N Latitude - Nome to Pt. Hope across Bering Strait										
HLY1203-A (October 7–12, 2012)	6.5	±	2.9	57	7.2	±	1.4	57	This Study	Yes
HLY1203-B (October 21–23, 2012)	4.9	±	1.4	34	8.1	±	1.3	34	This Study	Yes
RB1505-A (August 11–21, 2015)	32.8	±	38.6	24	7.3	±	1.4	23	This Study	Yes
RB1505-B (August 25–September 2, 2015)	15.7	±	7.4	25	6.2	±	0.8	25	This Study	Yes
SKQ2016-A (September 4–14, 2016)	17.0	±	7.3	43	10.0	±	1.9	43	This Study	Yes
SKQ2016-B (Septermber 16–26, 2016)	8.2	±	1.6	9	7.8	±	0.8	9	This Study	Yes
SKQ2017-A (August 7–9, 2017)	23.2	±	17.2	75	8.6	±	1.4	75	This Study	Yes
SKQ2017-B (August 10–22, 2017)	17.5	±	6.3	52	7.8	±	1.1	52	This Study	Yes
CHINARE - Open Water (July–September 2008)	25.9	±	9.6	6	n.m.	±	n.m.	n.a.	Yu et al., 2012	No
ICESCAPE - Open Water (June–July 2011)	43.7	±	29.5	15	8.3	±	2.1	15	Chaves et al., 2015	Yes
ICESCAPE - Open Water (June–July 2010)	26.6	±	10.1	4	7.9	±	1.5	4	Chaves et al., 2015	Yes
MR12-03 - Open Water (September–October 2012)	13.6	±	4.4	20	n.m.	±	n.m.	n.a.	Yamada et al., 2015	No
69–74 °N Latitude - Pt. Hope to north of Barrow										
HLY1203-A (October 7–12, 2012)	2.0	±	1.3	130	5.9	±	1.5	106	This Study	Yes
HLY1203-B (October 21–23, 2012)	1.9	±	1.9	101	7.7	±	2.6	74	This Study	Yes
RB1505-A (August 11–21, 2015)	10.0	±	6.1	67	6.7	±	1.1	67	This Study	Yes
RB1505-B (August 25–September 2, 2015)	13.0	±	4.3	35	6.7	±	0.9	35	This Study	Yes
SKQ2016-A (September 4–14, 2016)	5.8	±	2.7	185	7.9	±	1.0	185	This Study	Yes
SKQ2016-B (Septermber 16–26, 2016)	4.3	±	2.2	161	7.5	±	1.2	161	This Study	Yes
SKQ2017-A (August 7–9, 2017)	15.2	±	13.7	51	9.0	±	1.6	50	This Study	Yes
SKQ2017-B (August 10–22, 2017)	13.8	±	8.5	58	9.4	±	1.4	52	This Study	Yes
CHINARE - Open Water (July–September 2008)	15.9	±	7.1	18	n.m.	±	n.m.	n.a.	Yu et al., 2012	No
ICESCAPE < 10% ice cover (July 3–8, 2011)	10.7	±	3.0	10	7.1	±	1.8	10	Arrigo et al., 2012, 2014	Yes
ICESCAPE Under Ice Bloom > 50% ice cover (July 3–8, 2011)	42.7	±	22.8	20	9.6	±	4.1	20	Arrigo et al., 2012, 2014	Yes
SUBICE pre-Bloom (May–June 2014)	5.5	±	3.3	198	8.3	±	2.0	198	Arrigo et al., 2017	Yes
MR12-03 - Open Water (September–October 2012)	6.8	±	5.1	23	n.m.	±	n.m.	n.a.	Yamada et al., 2015	No

Avg., average; Sdev, standard deviation; n.m., not measured.

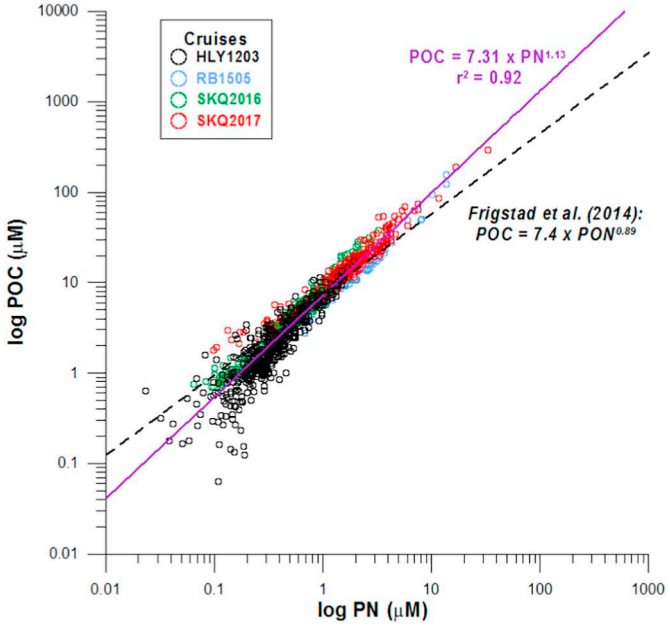

Fig. 14. Relationship between particulate nitrogen (PN) and particulate organic carbon (POC) concentrations for samples from the northern Bering and Chukchi Sea collected via surface underway system during the four cruises in this study (HLY1203, RB1505, SKQ2016 and SKQ2017). Included are the power fits to the data in this study (with 95% confidence intervals) and the global Arctic fit from Frigstad et al., 2014. (For interpretation of the references to color in this figure legend, the reader is referred to the web version of this article.)

measured at the Pt. Barrow met station (Fig. 2). In the case of the HLY1203 measurements, it is unlikely that sea ice melt water reached that far south (Weingartner et al., 2005; Danielson et al., 2017), so it is likely these salinity-temperature compositions reflect a pulse of modified water from another source (e.g., Kotzebue sound). In both cases, we suspect localized mixing may have led to nutrient injection into the surface layer and resulted in production of POM. The mechanisms for such mixing include interactions with bathymetry and coastlines which induce lateral intrusions, effects of internal waves and wind-driven turbulence on vertical fluxes, and shelf-break upwelling near Barrow Canyon (e.g., Pickart et al., 2013b; Rainville et al., 2011; Woodgate et al., 2015). These explanations are somewhat speculative at this point given the persistent and strong water column stratification that characterizes the western Arctic Shelf during this period (e.g., Danielson et al., 2017; Weingartner et al., 2017). Nevertheless, our results are consistent with other measurements, including elevated O_2/Ar values in surface waters, biologically-enhanced air-sea CO_2 flux and carbon deposition in underlying sediments (e.g., see Juranek et al., 2019; Grebmeier et al., 2015), all indicating these these locations as hot spots of production.

In general, samples from the BCSW displayed higher POC concentrations than their MW counterparts and displayed evidence of temporal variability. For example, samples with higher POC concentrations (> 16 μM) were measured during both August 2015 and 2017 (Fig. 16 b and d) relative to those in October 2012 and September 2016 (Fig. 16 a and c). Within BCSW, samples with higher salinity and temperature generally had higher POC values. In the case of the August 2015 data set, BCSW samples collected in the central area of the Chukchi Shelf (between Herald and Hannah Shoals) displayed significant increases in POC concentrations (see Fig. 8) following a storm event recorded at the Pt. Barrow met station in late August, when strong upwelling-favorable easterly winds with winds were followed by a rapid reversal and even stronger westerly winds that approached overall speeds of 30 knots (see Fig. 2). The suggestion is that the storm could have facilitated the mixing of nutrients (or POM) from deeper in the water column into surface waters, possibly resulting in enhanced productivity, elevated POC concentrations with close-to-Redifield [C:N]

Table 2
Compositional ranges of surface water masses from northern Bering Sea and Chukchi Sea region observed in this study.

Water Mass Name	Temperature	Salinity	Comments
	Range (°C)	Range	
Alaskan Coastal Water (ACW)	7 to 16	20 to 33	Temperature and salinity ranges extended from those in Danielson et al., 2017
Bering-Chukchi Winter Water (BCWW)	-2 to 0	30 to 33.5	Combination of Bering Shelf and Chukchi Shelf winter waters
Bering-Chukchi Summer Water (BCSW)	0 to 7	30 to 33.5	Combination of Bering Shelf and Chukchi Shelf summer waters
Sea ice Melt Water (MW)	-2 to 7	23 to 30	Extended to include a few samples with salinities lower than 25

Based on Danielson et al., 2017 with modifications described in comments.

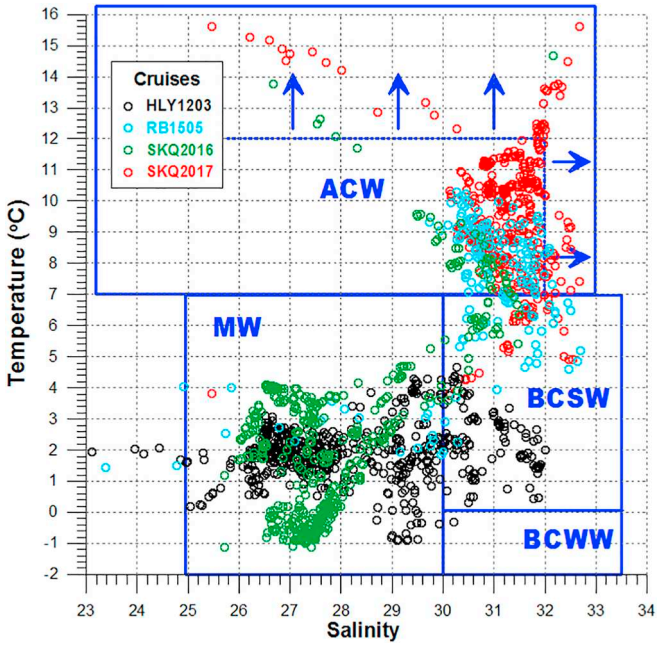

Fig. 15. Salinity vs. temperature plot for water samples from the northern Bering and Chukchi Sea collected via surface underway systems during the four cruises in this study (HLY1203, RB1505, SKQ2016 and SKQ2017). The ranges of the following water masses based on Danielson et al. (2017b) are indicated in the graph: Alaskan Coastal Water (ACW), Bering-Chukchi Winter Water (BCWW), Bering-Chukchi Summer Water (BCSW), and sea ice Melt Water (MW). The arrows indicate the expansion on the ACW's range from previously published limits. (For interpretation of the references to color in this figure legend, the reader is referred to the web version of this article.)

ratios (Fig. 11b). In the case of the August 2017 cruise, almost all of the high POC samples (16 to > 30 μM) were from the nearshore region east of Icy Cape and Utqiagvik and were collected on Aug 21–22, 2017 (Fig. 10). Examination of the wind records from Barrow Met station show a strong reversal in winds from downwelling favorable to upwelling favorable in the period between occupations (Fig. 2), suggesting the differences in POM standing stocks may be a response to wind-driven mixing.

Samples from ACW were collected during August 2015, August 2017 and September 2016. This water mass was characterized by the broadest range in POC concentrations, from low values < 6 μM to high values over 60 μM. It is clear from the distribution maps (Figs. 8–10), that the high variability in POC concentrations displayed by this water mass is related to coastal and frontal features that likely promote mixing and result in nutrient injection and enhanced production. Support for this hypothesis is provided by the fact that the highest concentrations were measured in a relatively narrow range of temperature (7–11 °C) and salinity (31 − 32) within the wider ACW compositional characteristics. Thus, our results indicate that colder waters within the ACW have the highest POC concentrations, which may be expected if mixing of deeper waters with elevated nutrients were responsible for extra production of autochthonous OM. The highly variable wind data from the Pt. Barrow met station (Fig. 2) and the satellite image from MODIS (Fig. 1) indicate this process has a degree of temporal variability and spatial surface expression that appears consistent with our observations. The lack of a trend with decreasing salinity suggests fluvial inputs of terrigenous POM are not contributing to the high POM levels during this period. On the other hand, the high variability in [C:N] ratios displayed by ACW samples (Fig. 11) makes it difficult to unambiguously determine whether or not coastal erosion and particle resuspension, which we expect would contribute POM with elevated [C:N] ratios, can explain the higher POC concentrations of specific samples from this water mass.

Table 3 summarizes the compositions of these water masses and presents the average and standard deviations of POC and PN concentrations as well molar [C:N] ratios as a function of season (August–October). Overall, these data suggest POM levels are consistently high along the ACW during the August–September period. Unlike BCSW and MW, we did not measure ACW samples in October, so we are unable to determine whether POM concentrations remain high later in the season. In the case of BCSW samples, it is clear that moderately elevated POM concentrations are found from August to September, with a significant decrease measured in October. In contrast, MW waters samples show a moderate drop in POC between September and October, with the high values measured in August 2015 being difficult to interpret due to the very few number of samples from this water mass (n = 8). Particulate nitrogen concentrations displayed overall similar trends to POC, whereas [C:N] ratios displayed variability that was largely unrelated to season.

7. Conclusions and future work

The combined use of surface underway systems with a semi-automated filtration system highlights the benefits and potential of high resolution particle collection. Our results show interesting spatial and temporal patterns in POM concentrations and compositions that are directly relatable to distinct water masses. Hence, much of the variability observed in POM along surface waters of the northern Bering and Chukchi shelves is to a large degree explained by the distribution of water masses during different periods. The high spatial resolution afforded by our approach provides clear evidence for the role of wind and physical features – such as straits, capes, fronts – in controlling the standing stocks of POM. The interactions of currents and fronts with bathymetric and coastline features appear to promote mixing of nutrients into the otherwise highly stratified and nutrient depleted surface waters that characterize the region during the late summer and fall. The increases in POC concentrations of a specific water mass prior and after a storm event in August 2015 provide evidence that events (through mixing and/or upwelling) may be able to inject nutrients into an otherwise highly stratified water column. Our overall conclusion is that all of these processes can act to promote moderate levels of localized productivity and maintain relatively high standing stocks of POM in surface waters through much of the open water season. Marked decreases in POM concentrations of some water masses later in the season are consistent with decreased production and export or degradation of

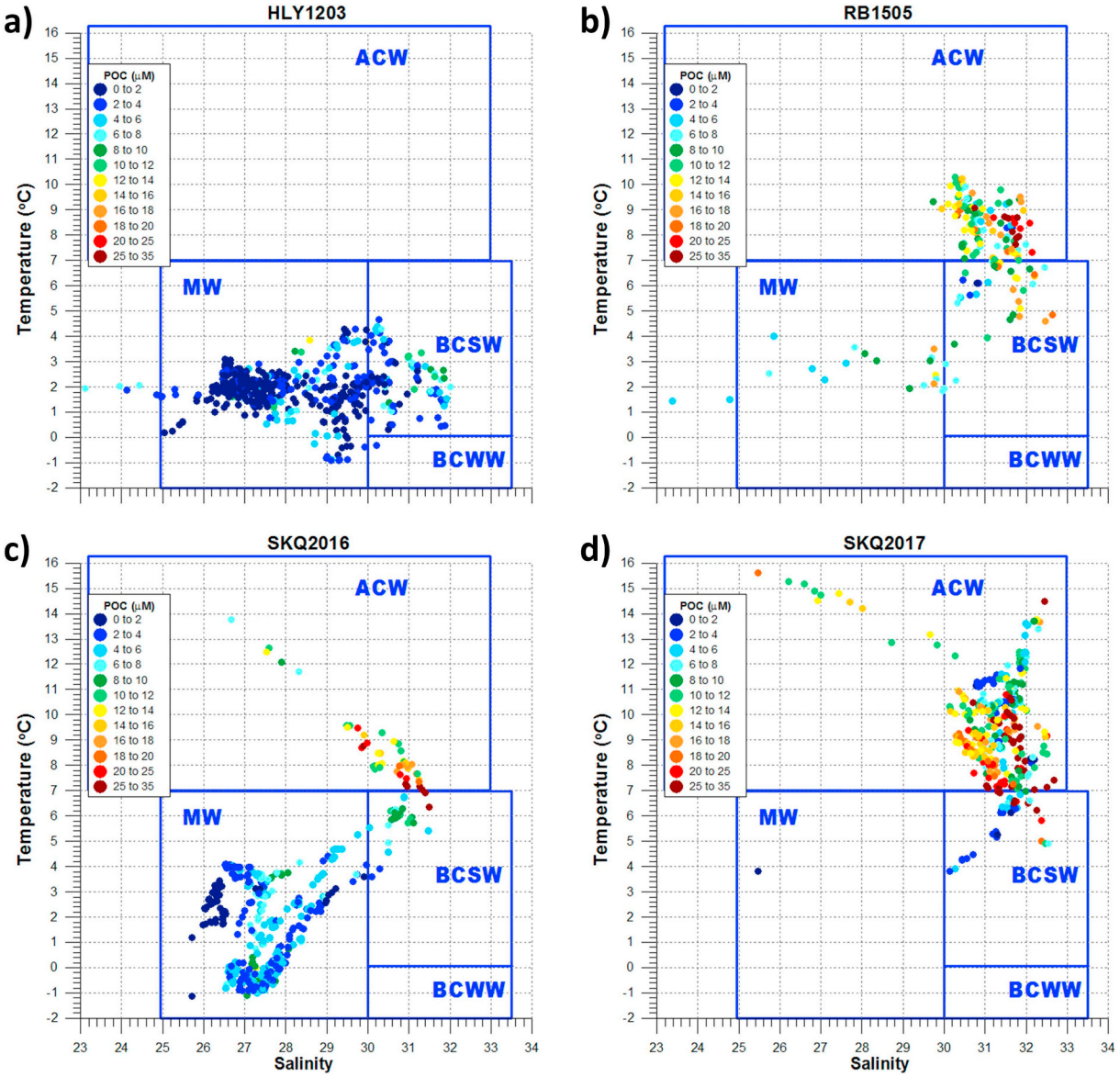

Fig. 16. Particulate organic carbon (POC) concentration data plotted in salinity-temperature graphs for water samples from the northern Bering and Chukchi Sea collected via surface underway systems during the following cruises: a) HLY1203, b) RB1505, c) SKQ2016 and d) SKQ2017. The ranges of the following water masses are indicated in each graph: Alaskan Coastal Water (ACW), Bering-Chukchi Winter Water (BCWW), Bering-Chukchi Summer Water (BCSW), and Sea ice Melt Water (MW) – see Fig. 15 for details. (For interpretation of the references to color in this figure legend, the reader is referred to the web version of this article.)

POM in surface waters.

More quantitative explanations for the observed trends in POM concentrations (and compositions) require additional data with similar spatial and temporal resolution. Examples of these types of data sets are continuous dissolved oxygen concentrations and dissolved oxygen saturation levels based on O_2/Ar measurements carried out with surface underway systems (e.g., Juranek et al., 2019). For example, dissolved oxygen saturation measurements can constrain net photosynthesis and respiration and thus help evaluate processes responsible for trends in POM concentrations. Furthermore, it may be possible to evaluate POM export by identifying regions and periods with elevated O_2/Ar ratios and low or decreasing POM concentrations. In addition, careful examination of vertical water column distributions in the study area are required to gain a more mechanistic understanding of the forcings and processes that may result in nutrient injection into otherwise nutrient-poor, highly stratified waters. These studies are currently being carried out as different data sets are fully analyzed and integrated. We expect this approach to be highly informative and used in future and on-going investigations of carbon dynamics of Arctic seas, including the development of temporal, spatial and water mass-specific algorithms that can be used for field calibrations of in-situ and remote sensor applications.

Acknowledgements and data availiability

Angel White, Katie Watkins-Brandt, Burke Hales and Rachel Holser are thanked for their contributions towards the development of the surface underway-SAFS application. Michael Wojahn, Kimberly Craig, Emmanuel Alegria and Erin Guillory helped sample collection. We thank HLY1203 co-chief scientists Robert Pickart and Jeremy Mathis and RB1505 chief scientists Nancy Kachel for providing opportunities to fully participate in all cruise activities. We also like to thank the captains and crew of all three vessels, including marine technicians

Table 3
Compositional ranges of surface water masses from northern Bering Sea and Chukchi Sea region observed in this study.

Water Mass	Aug-2017 SKQ2017	Aug-2015 RB1505	Sep-2016 SKQ2016	Oct-2012 HLY1203
POC (μM)				
ACW	19.3 ± 12.2 *(189)*	12.6 ± 6.3 *(78)*	14.1 ± 4.7 *(42)*	n.m.
BCSW	11.3 ± 15.7 *(41)*	12.4 ± 10.3 *(37)*	12.8 ± 9.4 *(31)*	4.6 ± 2.8 *(79)*
MW	n.m.	9.3 ± 4.1 *(8)*	4.0 ± 2.1 *(415)*	2.8 ± 2.4 *(177)*
PN (μM)				
ACW	2.20 ± 1.19 *(189)*	1.87 ± 0.83 *(78)*	1.48 ± 0.33 *(42)*	n.m.
BCSW	1.40 ± 2.14 *(41)*	1.88 ± 1.51 *(37)*	1.32 ± 0.72 *(31)*	0.63 ± 0.35 *(77)*
MW	n.m.	1.21 ± 0.40 *(8)*	0.53 ± 0.26 *(415)*	0.46 ± 0.33 *(177)*
[C:N] (mol:mol)				
ACW	8.7 ± 1.5 *(189)*	6.7 ± 1.0 *(78)*	9.5 ± 1.7 *(42)*	n.m.
BCSW	10.4 ± 4.0 *(41)*	6.6 ± 1.0 *(37)*	8.9 ± 1.8 *(31)*	7.5 ± 2.3 *(77)*
MW	n.m.	7.6 ± 1.1 *(8)*	7.5 ± 1.1 *(415)*	6.2 ± 2.4 *(177)*

POC, particulate organic carbon; PN, particulate nitrogen; [C:N], carbon:nitrogen ratio of particulate organic matter. For each water mass and cruise we report average ± standard deviation and number of samples (italics within parentheses); n.m., samples from that water mass not measured.

Steven Hartz, Erik Arnesen, Ethan Roth, and Bern McKiernan for their valuable help during all aspects of the work with the surface underway systems. Funding for this work was provided by U.S. National Science Foundation (NSF) Arctic Natural Sciences grant 1504394. All data presented are available at NSF's Arctic Data Center (https://arcticdata.io/) where they have been published (https://doi.org/10.18739/A27W67535).

Appendix A. Supplementary data

Supplementary data to this article can be found online at https://doi.org/10.1016/j.marchem.2019.03.010.

References

Anderson, L.G., Macdonald, R.W., 2015. Observing the Arctic Ocean carbon cycle in a changing environment. Polar Res. 34.
Ardyna, M., et al., 2014. Recent Arctic Ocean sea ice loss triggers novel fall phytoplankton blooms. Geophys. Res. Lett. 41 (17), 6207–6212.
Arrigo, K.R., 2015. Impacts of Climate on EcoSystems and Chemistry of the Arctic Pacific Environment (ICESCAPE). Deep-Sea Res. II Top. Stud. Oceanogr. 118 (Part A), 1–6.
Arrigo, K.R., van Dijken, G., Pabi, S., 2008. Impact of a shrinking Arctic ice cover on marine primary production. Geophys. Res. Lett. 35 (19).
Arrigo, K.R., et al., 2012. Massive phytoplankton blooms under Arctic Sea ice. Science 336 (6087), 1408.
Arrigo, K.R., et al., 2014. Phytoplankton blooms beneath the sea ice in the Chukchi sea. Deep Sea Res. II Top. Stud. Oceanogr. 105, 1–16.
Arrigo, K.R., et al., 2017. Late spring nitrate distributions beneath the ice-covered northeastern Chukchi shelf. J. Geophys. Res. Biogeosci. 122 (9), 2409–2417.
Balch, W.M., Bowler, B.C., Lubelczyk, L.C., Stevens, M.W., 2014. Aerial extent, composition, bio-optics and biogeochemistry of a massive under-ice algal bloom in the Arctic. Deep Sea Res. II Top. Stud. Oceanogr. 105, 42–58.
Baumgartner, M.F., Stafford, K.M., Winsor, P., StatScewich, F., Fratantoni, D.M., 2014. Glider-based passive acoustic monitoring in the Arctic. Mar. Technol. Soc. J. 48 (5), 40–51.
Behrenfeld, M.J., et al., 2017. Annual boom-bust cycles of polar phytoplankton biomass revealed by space-based lidar. Nat. Geosci. 10 (2), 118.
Cetinić, I., Poulton, N., Slade, W.H., 2016. Characterizing the phytoplankton soup: pump and plumbing effects on the particle assemblage in underway optical seawater systems. Opt. Express 24 (18), 20703–20715.
Chaves, J.E., et al., 2015. Assessment of ocean color data records from MODIS-Aqua in the western Arctic Ocean. Deep-Sea Res. II Top. Stud. Oceanogr. 118, 32–43 Part A.
Coachman, L.K., Aagaard, K., Tripp, B.W., 1975. Bering Strait: The Regional Physical Oceanography. University of Washington Press, Seattle.
Danielson, S.L., et al., 2014. Coupled wind-forced controls of the Bering-Chukchi shelf circulation and the Bering Strait throughflow: Ekman transport, continental shelf waves, and variations of the Pacific-Arctic sea surface height gradient. Prog. Oceanogr. 125, 40–61.
Danielson, S.L., et al., 2017. A comparison between late summer 2012 and 2013 water masses, macronutrients, and phytoplankton standing crops in the northern Bering and Chukchi Seas. Deep Sea Research Part II: Topical Studies in Oceanography 135, 7–26.
Fetterer, F., Knowles, K., Meier, W., Savoie, M., Windnagel, A.K., 2017. Sea Ice Index, Version 3. Sea Ice Extent and Concentration. NSIDC: National Snow and Ice Data Center, Boulder, Colorado USA. https://doi.org/10.7265/N5K072F8. updated daily. (September 5, 2018).
Forest, A., et al., 2011. Biogenic carbon flows through the planktonic food web of the Amundsen Gulf (Arctic Ocean): a synthesis of field measurements and inverse modeling analyses. Prog. Oceanogr. 91 (4), 410–436.
Forest, A., et al., 2014. Synoptic evaluation of carbon cycling in the Beaufort Sea during summer: contrasting river inputs, ecosystem metabolism and air-sea CO2 fluxes. Biogeosciences 11 (10), 2827–2856.
Frigstad, H., Andersen, T., Bellerby, R.G.J., Silyakova, A., Hessen, D.O., 2014. Variation in the seston C:N ratio of the Arctic Ocean and pan-Arctic shelves. J. Mar. Syst. 129, 214–223.
Gardner, W.D., Richardson, M.J., Carlson, C.A., Hansell, D., Mishonov, A.V., 2003. Determining true particulate organic carbon: bottles, pumps and methodologies. Deep Sea Res. II 50 (3–4), 655–674.
Goni, M.A., Teixeira, M.J., Perkeya, D.W., 2003. Sources and Distribution of Organic Matter in a River-Dominated Estuary (Winyah Bay, SC, USA). Estuarine, Coastal and Shelf Science. 56 (in press).
Goni, M.A., et al., 2006. The effect of Hurricane Lili on the distribution of organic matter along the inner Louisiana shelf (Gulf of Mexico, USA). Cont. Shelf Res. 26 (17–18), 2260–2280.
Goñi, M.A., White, A., Shearman, K., Lerczak, J., Wheatcroft, R., Hatten, J., 2017. The impact of riverine flooding on coastal biogeochemistry in the Pacific Northwest (Abstract ID: 29514). In: 2017 Aquatic Sciences Meeting - Mountains to the Sea, Honolulu, HI, 26 February to 3 March, 2017.
Grebmeier, J.M., Cooper, L.W., Feder, H.M., Sirenko, B.I., 2006. Ecosystem dynamics of the Pacific-influenced Northern Bering and Chukchi Seas in the Amerasian Arctic. In: Progress In Oceanography. Structure and Function of Contemporary Food Webs on Arctic Shelves: A Pan-Arctic Comparison. 71(2–4). pp. 331–361.
Grebmeier, J.M., Harvey, H.R., Stockwell, D.A., 2009. The Western Arctic Shelf-Basin Interactions (SBI) project, volume II: an overview. Deep Sea Res. II Top. Stud. Oceanogr. 56 (17), 1137–1143.
Grebmeier, J.M., et al., 2015. Ecosystem characteristics and processes facilitating persistent macrobenthic biomass hotspots and associated benthivory in the Pacific Arctic. Prog. Oceanogr. 136, 92–114.
Hauri, C., et al., 2018. From Sea Ice to Seals: A Moored Marine Ecosystem Observatory in the Arctic. submitted.
Holser, R.R., Goni, M.A., Hales, B., 2011. Design and application of a semi-automated filtration system to study the distribution of particulate organic carbon in the water column of a coastal upwelling system. Mar. Chem. 123 (1–4), 67–77.
Jackson, J.M., Allen, S.E., McLaughlin, F.A., Woodgate, R.A., Carmack, E.C., 2011. Changes to the near-surface waters in the Canada Basin, Arctic Ocean from 1993–2009: a basin in transition. J. Geophys. Res. 116 (C10), C10008.
Juranek, L.W., Hamme, R.C., Kaiser, J., Wanninkhof, R., Quay, P.D., 2010. Evidence of O-2 consumption in underway seawater lines: implications for air-sea O-2 and CO_2 fluxes. Geophys. Res. Lett. 37, L01601. https://doi.org/10.1029/2009gl040423.
Juranek, L., Takahashi, T., Mathis, J., Pickart, R., 2019. Significant biologically-mediated CO_2 uptake in the Pacific Arctic during the late open water season. J. Geophys. Res. Oceans. https://doi.org/10.1029/2018JC014568. in press.
McLaughlin, F.A., Carmack, E.C., 2010. Deepening of the nutricline and chlorophyll maximum in the Canada Basin interior, 2003–2009. Geophys. Res. Lett. 37 (24), L24602.

Moline, M.A., et al., 2008. High latitude changes in ice dynamics and their impact on polar marine ecosystems. In: Year in Ecology and Conservation Biology 2008. 1134. pp. 267–319.
Moran, S.B., Charette, M.A., Pike, S.M., Wicklund, C.A., 1999. Differences in seawater particulate organic carbon concentration in samples collected using small- and large-volume methods: the importance of DOC adsorption to the filter blank. Mar. Chem. 67 (1–2), 33–42.
Pabi, S., van Dijken, G.L., Arrigo, K.R., 2008. Primary production in the Arctic Ocean, 1998–2006. J. Geophys. Res. Oceans 113 (C8).
Pickart, R.S., et al., 2009. Upwelling on the continental slope of the Alaskan Beaufort Sea: storms, ice, and oceanographic response. J. Geophys. Res. Oceans 114.
Pickart, R.S., et al., 2011. Upwelling in the Alaskan Beaufort Sea: atmospheric forcing and local versus non-local response. Prog. Oceanogr. 88 (1–4), 78–100.
Pickart, R.S., et al., 2013a. Long-term trends of upwelling and impacts on primary productivity in the Alaskan Beaufort Sea. Deep Sea Res. I Oceanogr. Res. Pap. 79, 106–121.
Pickart, R.S., Spall, M.A., Mathis, J.T., 2013b. Dynamics of upwelling in the Alaskan Beaufort Sea and associated shelf-basin fluxes. Deep Sea Res. I Oceanogr. Res. Pap. 76, 35–51.
Rainville, L., Lee, C.M., Woodgate, R.A., 2011. Impact of wind-driven mixing in the Arctic Ocean. Oceanography 24 (3), 136–145.
Sterner, R.W., et al., 2008. Scale-dependent carbon : nitrogen: phosphorus seston stoichiometry in marine and freshwaters. Limnol. Oceanogr. 53 (3), 1169–1180.
Stigebrandt, A., 1984. The North Pacific: a global-scale estuary. J. Phys. Oceanogr. 14, 464–470.
Vaughan, D.G., et al., 2013. Observations: cryosphere. In: Stocker, T.F. (Ed.), The Physical Science Basis. Contribution of Working Group I to the Fifth Assessment Report of the Intergovernmental Panel on Climate Change. Cambridge University Press, Cambridge, United Kingdom and New York, NY, USA, pp. 317–382.
Weingartner, T., et al., 2005. Circulation on the north central Chukchi Sea shelf. Deep-Sea Res. II Top. Stud. Oceanogr. 52 (24–26), 3150–3174.
Weingartner, T., et al., 2017. The summer hydrographic structure of the Hanna Shoal region on the northeastern Chukchi Sea shelf: 2011–2013. Deep Sea Res. II Top. Stud. Oceanogr. 144, 6–20.
Welch, K., 2015. Analysis of Particulate Organic Matter Distribution along Surface Waters of the California Current. Honors College Thesis Thesis. Oregon State University.
Wood, K.R., et al., 2015. A decade of environmental change in the Pacific Arctic region. Prog. Oceanogr. 136, 12–31.
Woodgate, R.A., Weingartner, T.J., Lindsay, R., 2012. Observed increases in Bering Strait oceanic fluxes from the Pacific to the Arctic from 2001 to 2011 and their impacts on the Arctic Ocean water column. Geophys. Res. Lett. 39.
Woodgate, R.A., Stafford, K.M., Prahl, F.G., 2015. A synthesis of year-round interdisciplinary mooring measurements in the Bering Strait (1990–2014) and the RUSALCA years (2004–2011). Oceanography 28 (3), 46–67.
Wyatt, S.N., Crawford, D.W., Wrohan, I.A., Varela, D.E., 2013. Distribution and composition of suspended biogenic particles in surface waters across Subarctic and Arctic Seas. J. Geophys. Res. Oceans 118 (12), 6867–6880.
Yamada, Y., et al., 2015. Localized accumulation and a shelf-basin gradient of particles in the Chukchi Sea and Canada Basin, western Arctic. J. Geophys. Res. Oceans 120 (7), 4638–4653.
Yamamoto-Kawai, M., et al., 2009. Surface freshening of the Canada Basin, 2003–2007: river runoff versus sea ice meltwater. J. Geophys. Res. Oceans 114.
Yu, W., He, J., Li, Y., Lin, W., Chen, L., 2012. Particulate organic carbon export fluxes and validation of steady state model of Th-234 export in the Chukchi Sea. Deep Sea Res. II Top. Stud. Oceanogr. 81-84, 63–71.
Zhang, J.L., et al., 2010. Modeling the impact of declining sea ice on the Arctic marine planktonic ecosystem. J. Geophys. Res. Oceans 115.